Global Biogeochemical Cycles

RESEARCH ARTICLE
10.1029/2022GB007466

**Key Points:**

- Shelf sediments release redox-sensitive trace metals (TMs) to overlying oxygen-depleted waters in the Benguela Upwelling System
- Sediment-derived TMs are upwelled and laterally transported constituting a major source to shelf waters and to the eastern South Atlantic
- Subsurface fluxes of dissolved Fe and Co from the shelf edge play an important role in supplying Fe and Co to the eastern South Atlantic

**Supporting Information:**

Supporting Information may be found in the online version of this article.

**Correspondence to:**

T. Liu and R. C. Xie,
tliu@geomar.de;
ruifang.xie@sjtu.edu.cn

**Citation:**

Liu, T., Krisch, S., Xie, R. C., Hopwood, M. J., Dengler, M., & Achterberg, E. P. (2022). Sediment release in the Benguela Upwelling System dominates trace metal input to the shelf and eastern South Atlantic Ocean. *Global Biogeochemical Cycles*, *36*, e2022GB007466. https://doi.org/10.1029/2022GB007466

Received 20 MAY 2022
Accepted 15 SEP 2022

**Author Contributions:**

**Conceptualization:** Te Liu, Ruifang C. Xie, Mark J. Hopwood, Eric P. Achterberg
**Formal analysis:** Te Liu, Stephan Krisch, Mark J. Hopwood, Marcus Dengler
**Software:** Te Liu
**Visualization:** Te Liu
**Writing – original draft:** Te Liu
**Writing – review & editing:** Te Liu, Stephan Krisch, Ruifang C. Xie, Mark J. Hopwood, Marcus Dengler, Eric P. Achterberg



# Sediment Release in the Benguela Upwelling System Dominates Trace Metal Input to the Shelf and Eastern South Atlantic Ocean

**Te Liu[1], Stephan Krisch[1,2], Ruifang C. Xie[1,3], Mark J. Hopwood[1,4], Marcus Dengler[1], and Eric P. Achterberg[1]**

[1]GEOMAR Helmholtz Centre for Ocean Research Kiel, Kiel, Germany, [2]Now at Bundesanstalt für Gewässerkunde, Koblenz, Germany, [3]School of Oceanography, Shanghai Jiao Tong University, Shanghai, China, [4]Department of Ocean Science and Engineering, Southern University of Science and Technology, Shenzhen, China

**Abstract** Upwelling of subsurface waters injects macronutrients (fixed N, P, and Si) and micronutrient trace metals (TMs) into surface waters supporting elevated primary production in Eastern Boundary Upwelling Regions. The eastern South Atlantic features a highly productive shelf sea transitioning to a low productivity N-Fe (co)limited open ocean. Whilst a gradient in most TM concentrations is expected in any off-shelf transect, the factors controlling the magnitude of cross-shelf TM fluxes are poorly constrained. Here, we present dissolved TM concentrations of Fe, Co, Mn, Cd, Ni, and Cu within the Benguela Upwelling System from the coastal section of the GEOTRACES GA08 cruise. Elevated dissolved Fe, Co, Mn, Cd, Ni, Cu and macronutrient concentrations were observed near shelf sediments. Benthic sources supplied 2.22 ± 0.99 μmol Fe $m^{-2}$ $day^{-1}$, 0.05 ± 0.03 μmol Co $m^{-2}$ $day^{-1}$, 0.28 ± 0.11 μmol Mn $m^{-2}$ $day^{-1}$ and were found to be the dominant source to shallow shelf waters compared to atmospheric depositions. Similarly, off-shelf transfer was a more important source of TMs to the eastern South Atlantic Ocean compared to atmospheric deposition. Assessment of surface (shelf, upper 200 m) and subsurface (shelf edge, 200–500 m) fluxes of Fe and Co indicated TM fluxes from subsurface were 2–5 times larger than those from surface into the eastern South Atlantic Ocean. Under future conditions of increasing ocean deoxygenation, these fluxes may increase further, potentially contributing to a shift toward more extensive regional limitation of primary production by fixed N availability.

## 1. Introduction

Trace metals (TM) including iron (Fe), cobalt (Co), manganese (Mn), cadmium (Cd), nickel (Ni) and copper (Cu) participate in a range of cellular processes that play a key role in phytoplankton growth and marine primary productivity (Twining & Baines, 2013). Marine phytoplankton growth is often limited by the availability of macronutrients (nitrogen [N], phosphorus [P], and silicic acid [Si]) or the micronutrient Fe (Hutchins & Bruland, 1998; Moore et al., 2013). Cobalt and Mn (co)limitation of marine phytoplankton growth has also been experimentally identified by in-lab culture and ship-board measurements (Browning et al., 2017, 2021; Saito et al., 2002; Wu et al., 2019).

The Benguela Upwelling System (BUS) off the Namibian shelf is the most productive one and has the highest carbon export of the four Eastern Boundary Upwelling Regions (EBUR) (Carr, 2001). The upwelling of macronutrient-rich subsurface waters from the thermocline and on-shelf regeneration of nutrients in the euphotic zone of the BUS stimulates high phytoplankton growth (Dittmar & Birkicht, 2001; Flynn et al., 2020).The subsequent sinking and remineralization of particulate organic matter depletes subsurface water oxygen concentrations which, in combination with poor ventilation in the subsurface, creates an oxygen minimum zone (OMZ, defined herein as oxygen <100 μmol $kg^{-1}$) in the thermocline of the EBUR (Karstensen et al., 2008; Monteiro & van der Plas, 2006). Low oxygen concentrations overlying shelf sediments favor the release of redox-sensitive TMs (e.g., Fe, Co and Mn) (Homoky et al., 2012; Rapp et al., 2020) and alleviate Fe depletion relative to macronutrients in the upwelled waters, particularly where the shelf is broad (>80 km) (Bruland et al., 2005; Johnson et al., 1999; Lohan & Bruland, 2008; Moore et al., 2013). The input of shelf sediment-derived micronutrients such as Fe to overlying waters is therefore critical for determining the identity of the (micro)nutrient proximally constraining primary production in OMZ regions (Browning et al., 2017, 2018). Yet quantifying how vertical and lateral fluxes of TMs scale with benthic release into the water column remains a key challenge in assessing to what extent

OMZ expansion or contraction may be mediated by biogeochemical feedbacks (Landolfi et al., 2013; Wallmann et al., 2022). Observations regarding transport of TMs across shelf to the open ocean in OMZ regions are sparse limiting our understanding of the underlying processes defining spatial/temporal trends in TM (co)-limitation of primary production. The only study reported radium-derived TM fluxes across the shelf from the Peruvian OMZ also noted high uncertainty on the fluxes due to low sampling resolution and strong spatial variability in radium and TM concentrations (Sanial et al., 2018).

Here we present depth profiles of dissolved Fe, Co, Mn, Cd, Ni, and Cu and macronutrient concentrations within the BUS as part of the GEOTRACES eastern South Atlantic Ocean GA08 cruise. The aim of this study was to quantify vertical and off-shelf fluxes of TMs to shelf surface waters and the eastern South Atlantic Ocean, and assess the relative importance of shelf sediment TMs sources on a regional scale.

## 2. Study Area

In the eastern South Atlantic Ocean, the poleward Angola Current and the equatorward Benguela Current converge at around ~15°S–17°S forming the Angola-Benguela Front. This divides the BUS into the Angola subtropical system in the north and the nutrient-rich BUS in the south (Jarre et al., 2015; Shillington et al., 2006; Stramma & Mathew, 1999). The Angola-Benguela Front and the southern tip of Africa (~35°S) thus mark the northern and southern boundaries of the BUS, respectively (Curl & Hill, 1964) (Figure 1). The Benguela Current originates from two primary sources: the South Atlantic Current flowing from west to east as part of the South Atlantic subtropical gyre, and water flowing equatorward originating from the Agulhas Current (Garzoli & Gordon, 1996; Mercier et al., 2003).

Coastal upwelling in the BUS is wind-driven. Alongshore equatorward winds driving offshore Ekman transport of surface waters, and wind stress curl driving Ekman suction near the coast, lead to cool and macronutrient-rich

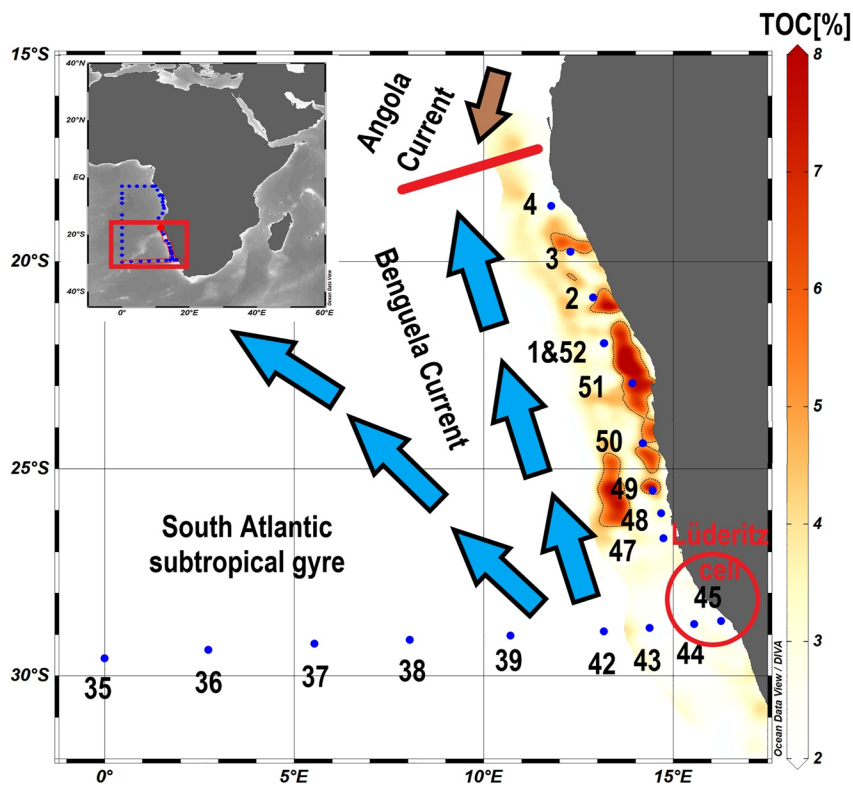


**Figure 1.** Map of the study area. Panel on the left corner shows the whole GA08 cruise track and the red square shows our study area. Sample locations for trace metals are marked by blue dots with station numbers. Blue and brown arrows and the red circle indicate the Benguela Current, the Angola Current and Lüderitz cell, respectively (Hutchings et al., 2009; Shillington et al., 2006). The yellow-red shading refers to the Total Organic Carbon (TOC) content (wt%) of the surface sediments (TOC data is from Inthorn et al., ; Schlitzer, 2020).

central water masses being upwelled to the surface (Bordbar et al., 2021; Nelson et al., 1996; Rae, 2005). Upwelled water masses include macronutrient-rich and oxygen-depleted South Atlantic Central Water (SACW) and the well-oxygenated Eastern SACW (200–300 µM oxygen) (Liu & Tanhua, 2021; Rae, 2005). Wind-driven upwelling creates several distinct upwelling cells along the BUS coastline, of which the Kunene (18°S) and Lüderitz (27°S) cells are the most vigorous with high offshore advection and strong turbulent mixing (Bordbar et al., 2021; Hutchings et al., 2009). Our study region from ~17°S to 29°S has year-round upwelling while further south upwelling has a seasonal maximum during austral spring and summer, and weakens sharply in winter due to a seasonal change in wind direction and strength (Hutchings et al., 2009). This drives a hotspot of primary production (~976 g C $m^{-2}$ $yr^{-1}$) for the BUS (Chavez & Messié, 2009).

The OMZ across the Namibian shelf results from a combination of oxygen consumption due to remineralization and southward advection of oxygen poor tropical waters (Mohrholz et al., 2008; Monteiro & van der Plas, 2006). The core of the coastal OMZ within our study area is at ~23°S–26°S at depths of ~100–200 m. Oxygen concentrations are perennially <90 µmol $kg^{-1}$ along the shelf and periodically suboxic (defined here as <20 µmol $kg^{-1}$) during late austral summer to autumn due to poleward advection of SACW by the poleward under current situated on the shelf and the upper continental slope (Junker et al., 2017; Mohrholz et al., 2008).

## 3. Materials and Methods

### 3.1. Seawater Sampling and Analysis

#### 3.1.1. Dissolved Trace Metal Seawater Sampling

Seawater samples for dissolved TMs were collected on RV Meteor cruise M121 (GEOTRACES GA08) in the period 22 November to 27 December 2015 (late spring and early austral summer). This study focuses on samples in the BUS within the GA08 section between 17°S and 29°S (Figure 1). For contamination prone parameters, seawater was sampled using trace metal clean GO-FLO bottles (Ocean Test Equipment, OTE) on a powder coated aluminum CTD (Sea-Bird SBE25) rosette frame (denoted the TM-CTD), which was deployed using a Kevlar conducting cable. At Stations 1 and 2, single GO-FLO bottles were instead deployed on an aramid line because of a pronounced (4–5 m) swell preventing the deployment of the TM-CTD. Upon recovery of the TM-CTD, the GO-FLO bottles were moved to a custom-made clean laboratory container, where they were over-pressurized by filtered ~1.2 atm $N_2$ and seawater was subsampled through 0.8/0.2 µm cartridge filters (AcroPak® 1000) into 125 ml acid-clean, low density polyethylene (LDPE) bottles (Nalgene®). The Acropack filters were re-used between samples. New filters were flushed with at least 10 L of surface seawater, and always with at least 500 mL of the sample prior to sampling. The LDPE bottles and all plasticware for sample handling was pre-cleaned in a 3-stage process (1 day in Mucasol detergent, 1 week in 1.2 M HCl and 1 week in 1.2 M $HNO_3$) with 3 rinses of MQ water between each stage. The filtered seawater samples were acidified to pH 1.9 via addition of 180 µL ultra-pure concentrated HCl (UpA grade, Romil®), double bagged in LDPE plastic bags and stored upright in the dark until analysis.

#### 3.1.2. Dissolved Trace Metal Analysis

UV-digested seawater samples were pre-concentrated off-line in a clean laboratory (ISO5) at GEOMAR using a WAKO chelate resin (Wako Pure Chemical Industries, Japan) on a seaFAST system (SC-4 DX SeaFAST pico, Elemental Scientific Inc.) exactly as in Rapp et al. (2017). Calibration was carried out via isotope dilution for Fe, Ni, Cu, and Cd, and standard additions for Mn and Co. Sample and reagent handling was performed within the same laboratory in an ISO 3 laminar flow bench with a HEPA filter unit. All reagents were prepared in MQ water (18.2 MΩ cm) (Cutter et al., 2017). Nitric acid was distilled in house (Savillex DST 1000). High purity glacial acetic acid and ammonium hydroxide (Optima, Fisher Scientific) were used to prepare ammonium acetate buffer (pH 8.5). Each pre-concentrated sample was analyzed for TMs concentrations on a high-resolution inductively coupled plasma mass spectrometer (HR-ICP-MS, ELEMENT XR, ThermoFisher Scientific). Data reported herein has been corrected for total procedural blanks (defined as manifold blanks plus buffer blanks) (Rapp et al., 2017). Certified reference seawater materials SAFe S, SAFe D2, GSP, and GSC were routinely analyzed alongside seawater samples (Tables S1 and S2 in Supporting Information S1).

#### 3.1.3. Macronutrient and Physical Parameter Analysis

Macronutrients sampled from the TM-CTD were analyzed for nitrate and nitrite (in the following termed $NO_x$), phosphate ($PO_4^{3-}$) and silicic acid ($Si(OH)_4$) on board by segmented flow injection analysis using a QUAATRO

(Seal Analytical) auto-analyzer following (Grasshoff et al., 1999). A non-trace metal clean CTD system was deployed on a steel cable at each station. Oxygen, temperature, salinity, and depth were measured with sensors (Seabird) on the stainless steel CTD that was deployed alongside the TM rosette.

### 3.1.4. Fe(II) Concentration Analysis

Unfiltered samples for Fe(II) were collected from trace metal clean GO-FLO bottles into opaque acid-cleaned high density polyethylene bottles. Fe(II) analysis was carried out in a laminar flowhood with a HEPA filter within 90 min of subsampling of the GO-FLO bottles and in the order of the sample collection (deepest sample first). Fe(II) was determined via flow injection analysis on a modified FeLume system using luminol chemiluminescence without preconcentration (Croot & Laan, 2002; Hopwood et al., 2017). Calibration via standard addition was conducted at each station on the same analytical run as samples. Peak heights from at least three peaks at 1 min intervals were used to calibrate the sample concentrations. The chemiluminescent response of luminol over broad ranges of Fe(II) concentration is non-linear which limits the calibration range at each station that can be made without adjusting the instrument sensitivity or diluting samples (which is analytically impractical given the sensitivity of Fe(II) decay to temperature, pH and dissolved oxygen). At stations with sharply elevated concentrations in the deepest samples a few Fe(II) concentrations (7 out of 51 total for the data herein) were beyond the highest standard addition (20 nM) and are therefore reported as >20 nM.

## 3.2. Flux Calculations

For flux calculations, the water column was divided into two layers separated by the upper boundary of the OMZ (Figure 2, density anomaly of ~26.5 kg $m^{-3}$). These two layers are referred to as the surface layer and the shelf bottom layer in the following text. We are primarily interested in the upwelling flux of TMs from the shelf

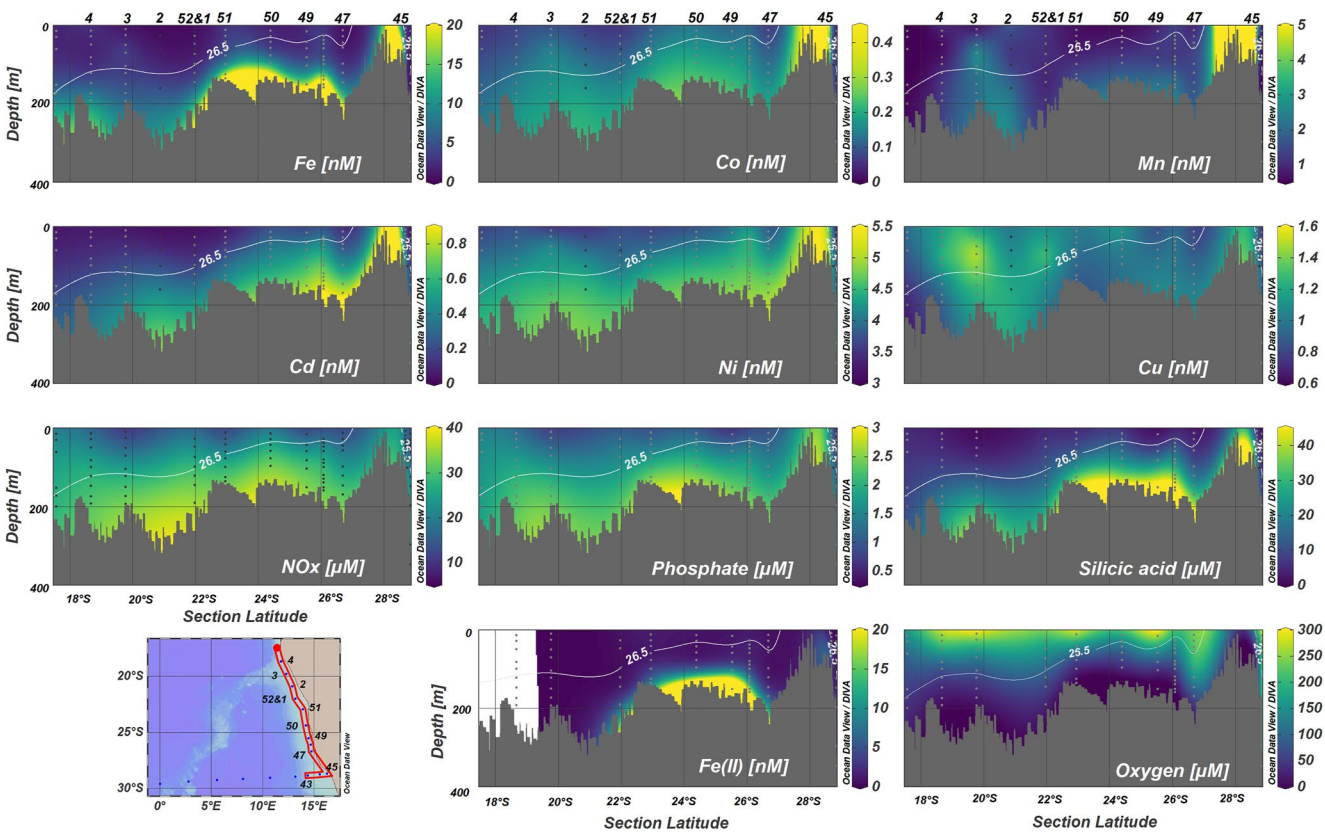


**Figure 2.** Shelf section plots of dissolved trace metals, Fe(II), $NO_x$ (nitrate + nitrite), oxygen, silicic acid and phosphate along the African coast for cruise M121. White contour lines overlaying each panel indicate the 26.5 kg $m^{-3}$ isopycnal over the shelf. Station numbers are indicated on top of figures and the bottom left panel. Figures were produced using Ocean Data View (Schlitzer, 2020).

bottom layer to the surface layer, and the subsequent alongshore (northward) and offshore (westward) fluxes in the surface layer.

#### 3.2.1. Vertical Fluxes

Vertical TM fluxes result from vertical diffusive and wind-induced advective transfer. Here, we focus on the vertical transfer across the 26.5 kg $m^{-3}$ isopycnal, which is at depths of 20–50 m for shelf region. The vertical TM flux ($J_z$, μmol $m^{-2}$ $day^{-1}$) is described as (Jickells, 1999):

$$J_z = K_z \frac{\partial [TM]}{\partial z} + w \cdot \Delta [TM] \tag{1a}$$

where $K_z$ is the turbulent diffusion coefficient ($m^2$ $s^{-1}$), $\partial [TM]/\partial z$ the vertical TM concentration gradient across the 26.5 kg $m^{-3}$ isopycnal (μmol $m^{-4}$), $w$ is upwelling velocity (m $s^{-1}$) at the base of 26.5 kg $m^{-3}$. $\Delta [TM]$ denotes trace metal concentration difference between the 26.5 kg $m^{-3}$ isopycnal and 10 m below this horizon in units of μmol $m^{-3}$ (Rapp et al., 2019; Steinfeldt et al., 2015).

Vertical turbulent diffusion coefficient ($K_z$) could not be determined from data collected during the cruise. An estimated $K_z$ of 1.0–1.7 × $10^{-4}$ $m^2 \cdot s^{-1}$ below the mixed layer at ~40°S of the South Atlantic Ocean was obtained in a previous study (Hsieh et al., 2021). Model-derived $K_z$ is broadly within the range of $10^{-6}$–$10^{-4}$ $m^2$ $s^{-1}$ below the mixed layer based on temperature microstructure observations (Dunckley et al., 2012). We thus consider a $K_z$ of $10^{-4}$ $m^2$ $s^{-1}$ a reasonable value to use in our calculations.

For vertical advective flux quantification, the upwelling velocity ($w'$) at the base of the mixed layer (determined by a change in potential density $\Delta\sigma_\theta$ = 0.125 kg $m^{-3}$) (Monterey & DeWitt, 2000) can be derived directly from the wind stress curl using Equations 1b–1c (see e.g., Bordbar et al., 2021; Gill & Adrian, 1982). Approximating a linear vertical decay of $w'$ that declines to zero at the ocean floor, we interpolated an upwelling velocity ($w$) for all stations along the Namibian shelf where the 26.5 kg $m^{-3}$ isopycnal is deeper than the mixed layer.

$$w' = -\frac{2\tau_y}{\rho f L_r} e^{2x/L_r} \tag{1b}$$

$$\tau_y = \rho_{\text{air}} C_D \lceil U \rceil U_y \tag{1c}$$

$\tau_y$ is the alongshore wind stress (N $s^{-2}$), $\rho$ the density of seawater (1,025 kg $m^{-3}$), $f$ the Coriolis parameter as a function of latitude ($s^{-1}$), $x$ the distance from maximum Ekman divergence taken here as the position at 50 m isobath on the shelf. The first baroclinic Rossby radius ($L_r$, km) here used is 35 km (Chelton et al., 1998).

The monthly alongshore wind stress ($\tau$) was calculated within 60 nautical miles of the coast based on monthly wind speed magnitude ($\lceil U \rceil = \sqrt{U_x^2 + U_y^2}$, m $s^{-1}$) and alongshore wind speed ($U_y$, m $s^{-1}$) using Equation 1c (Steinfeldt et al., 2015), where $\rho_{\text{air}}$ represents the density of air (1.225 kg $m^{-3}$) and $C_D$ is drag coefficient defined as 1.15 × $10^{-3}$ here (Fairall et al., 2003). The monthly satellite scatterometer wind speed data set is from Satellite Data Processing, Archiving and Distribution Center Satellitaire (CERSAT) at IFREMER, Plouzané (France) (file number 2015120100_2016010100_monthly-ifremer-L3-MWF-GLO-20160107162117-01.0). Our estimated upwelling velocities ($w'$) were generally on the order of $10^{-5}$ m $s^{-1}$ except a maximum upwelling velocity ($w'$) of 1.5 × $10^{-4}$ m $s^{-1}$ determined at Station 47 of 26.7°S, corresponding to the most vigorous Lüderitz cells where modeled upwelling rate was ~1.5 × $10^{-4}$ m $s^{-1}$ previously (Veitch et al., 2010). Due to uncertainties in the satellite wind product near the coast, we thus assume an error of 50% for the upwelling velocities (Rapp et al., 2019; Verhoef et al., 2012).

#### 3.2.2. Shelf-to-Ocean Trace Metal Fluxes

The lateral off-shelf TM fluxes were calculated using the following one-dimension model (De Jong et al., 2012; Glover et al., 2011):

$$\frac{\partial TM}{\partial t} = -u \left( \frac{\partial TM}{\partial x} \right) + K_x \left( \frac{\partial^2 TM}{\partial x^2} \right) + J_x \tag{2a}$$

where $u$ is cross-shelf velocity (m $s^{-1}$), $K_x$ is off-shelf diffusive coefficient ($m^2$ $s^{-1}$), $\partial TM/\partial x$ is off-shelf gradient (nmol $L^{-1}$ $m^{-1}$) in TM concentrations (nmol $L^{-1}$), $\partial^2 TM/\partial x^2$ (nmol $L^{-1}$ $m^{-2}$) is the second derivative of the TM concentration distribution with respect to the distance to the coast, and $J_x$ represents source/sink processes. We assume steady state ($\partial TM/\partial t = 0$), and Equation 2a can then be rearranged as:

$$J_x = u\left(\frac{\partial TM}{\partial x}\right) - K_x\left(\frac{\partial^2 TM}{\partial x^2}\right) \tag{2b}$$

Thus, the off-shelf flux divergence (μmol $m^{-3}$ $s^{-1}$) can be derived by Equation 2b because lateral flow in and out of the surface layer is the same under steady state. The depth of the surface layer (50 m at shelf stations, 200 and 500 m at open ocean stations) multiplied by the off-shelf flux divergence (μmol $m^{-3}$ $s^{-1}$) yields the lateral off-shelf flux (μmol $m^{-2}$ $day^{-1}$).

Cross-shelf velocities ($u$, m $s^{-1}$) that represent the real advection offshore were determined by zonal velocities continuously measured throughout the cruise using a vessel-mounted phased-array acoustic Doppler current profiler (75 kHz RDI Ocean Surveyor) and the shoreline orientation angle (21.4° from north) (Bordbar et al., 2021; Mohrholz et al., 2014). Velocities measured in the surface layer within 1° radius for stations were averaged and showed a generally off-shelf direction with $u$ ranging from 0.22 m $s^{-1}$ on the shelf to 0.03 m $s^{-1}$ in the open ocean. Taking a similar approach as in De Jong et al. (2012), the TM gradient is defined by the first derivative of the fitting power function of Fe, Co and Mn and the distance from the coast ($m$). The off-shelf diffusive coefficient $K_x$ was calculated from the empirical relationship $K_x = 0.0103\,l^{1.15}$ (Okubo, 1971), where the scale length ($l$ in m) was defined as the distance that TM concentration decreases to $1/e$ of its initial concentration (Johnson et al., 1997). In our calculations, $K_x$ was within the range of $10^3$ to $10^5$ $m^2$ $s^{-1}$.

#### 3.2.3. Alongshore Fluxes

The Benguela Current and the poleward undercurrent are well known advections governing the alongshore transportation of water masses (Peterson & Stramma, 1991; Shillington et al., 2006; Veitch et al., 2010). Here, we use underway current velocity data from cruise M121 to calculate the alongshore flux as:

$$J_y = \int_0^z v\frac{\partial[TM]}{\partial y}\mathrm{d}z \tag{3}$$

where $v$ is the alongshore velocity (m $s^{-1}$), $\partial[TM]/\partial y$ is the alongshore TM concentration gradient (nmol $L^{-1}$ $m^{-1}$), and $z$ is the depth interval ($m$) of interest (here 50 m was used, approximately the depth of our defined surface layer).

Alongshore velocity ($v$, m $s^{-1}$) was obtained by zonal and meridional velocities from the same acoustic Doppler current profilers (VMADCP; 75 kHz RDI Ocean Surveyor) and shoreline orientation angle with respect to the north (21.4°) (Bordbar et al., 2021). Velocities measured within 0.1° radian at shelf stations for the surface layer were averaged, resulting in an average equatorward alongshore current velocity of the surface layer of 0.008 m $s^{-1}$. Alongshore TM gradients were estimated from the difference in mean TM concentrations obtained by grouping stations and averaging TM concentrations within the surface layer on 1° × 1° grids.

## 4. Results and Discussions

### 4.1. Dissolved Trace Metal and Macronutrient Distributions

Concentrations of macronutrients including $NO_x$, $PO_4^{3-}$ and $Si(OH)_4$ were depleted in surface waters on the Namibian shelf and increased with depth (Figure 2). This trend was also observed for dissolved Fe, Fe(II), Co, Cd and Ni, due to release from shelf sediments interacting with the OMZ waters (Plass et al., 2021), biological drawdown in near-surface waters and remineralization at depth (Bruland et al., 2014). The highest concentrations of dissolved Fe, Fe(II) and Co were observed in near-bottom waters, reaching concentrations of 5.04–46.3 nM Fe, >20 nM Fe(II) and 0.19–0.44 nM Co, comparable to previous observations of Fe (7.9 nM) and Co (0.2 nM) for the same shelf area (Noble et al., 2012). Extremely high Fe concentrations in our study were similar to observations from the OMZ on the Peruvian shelf where bottom Fe concentrations over 30 nM have been observed (Bruland et al., 2005; Rapp et al., 2020). Enhanced concentrations of dissolved Mn were observed in near-bottom waters, but the maximum Mn concentration (16.2 nM) was observed in surface waters likely due to photo-reduction of Mn(IV) oxides to Mn(II) by sunlight coupled to an increased stability of Mn(II) (Sunda et al., 1983). For dissolved

Cd, Ni and Cu, maximum concentrations were typically in bottom waters. Subsurface maxima at several stations (e.g., Station 1–3 and 48) suggests an intense subsurface remineralization of sinking organic matter with release of the nutrient-type trace elements (Biller & Bruland, 2013). The southernmost, and shallowest station, (Station 45) exhibited the highest Fe, Co, Mn concentrations (Mn, highest in surface and second highest in bottom waters) for the Namibian shelf (Figures 1 and 2).

Compared to offshore stations, the most striking feature of TM distributions on the Namibian shelf was the enhanced concentrations in the OMZ, for example, dissolved Fe, Co and Mn concentrations consistently over 1.5 nM, 0.1 and 1 nM, respectively (Figures 2 and 3). Similarly, enhanced concentrations of Fe, Co, and Mn have been observed near our study area in the South Atlantic Ocean (Noble et al., 2012). Other EBUR including Mauritania, California and Peru also present enhanced Fe, Co, and Mn concentrations within the OMZ (Biller & Bruland, 2013; Rapp et al., 2019; Sanial et al., 2018). In contrast, $PO_4^{3-}$, silicic acid, dissolved Cd, Ni and Cu were less enhanced along the shelf, demonstrating a much smaller influence of low oxygen waters on these elements but a key driver on high concentrations of dissolved Fe, Co and Mn.

In the upper ocean along the shelf-to-open ocean transect at ~29°S, there was a sharp decrease in concentrations of Fe and Co moving off shelf (Figure 3). Conversely, distributions of dissolved Cd, Ni, and Cu are lack of this features. The rapid decrease of Fe suggests an efficient removal of Fe by scavenging (Boyd & Ellwood, 2010; Noble et al., 2012). Despite depleted Co in offshore surface water, relatively high Co concentrations were observed in subsurface water within the shelf plume (Figure 3), in agreement with observations along a zonal transect of the Peru upwelling system (Hawco et al., 2016; Sanial et al., 2018). There was also a persistent Mn maximum in offshore surface waters likely resulting from a combination of atmospheric deposition (Baker et al., 2006), photo-reduction (Sunda et al., 1983) and more efficient lateral transport of shelf sourced Mn than either Fe or Co

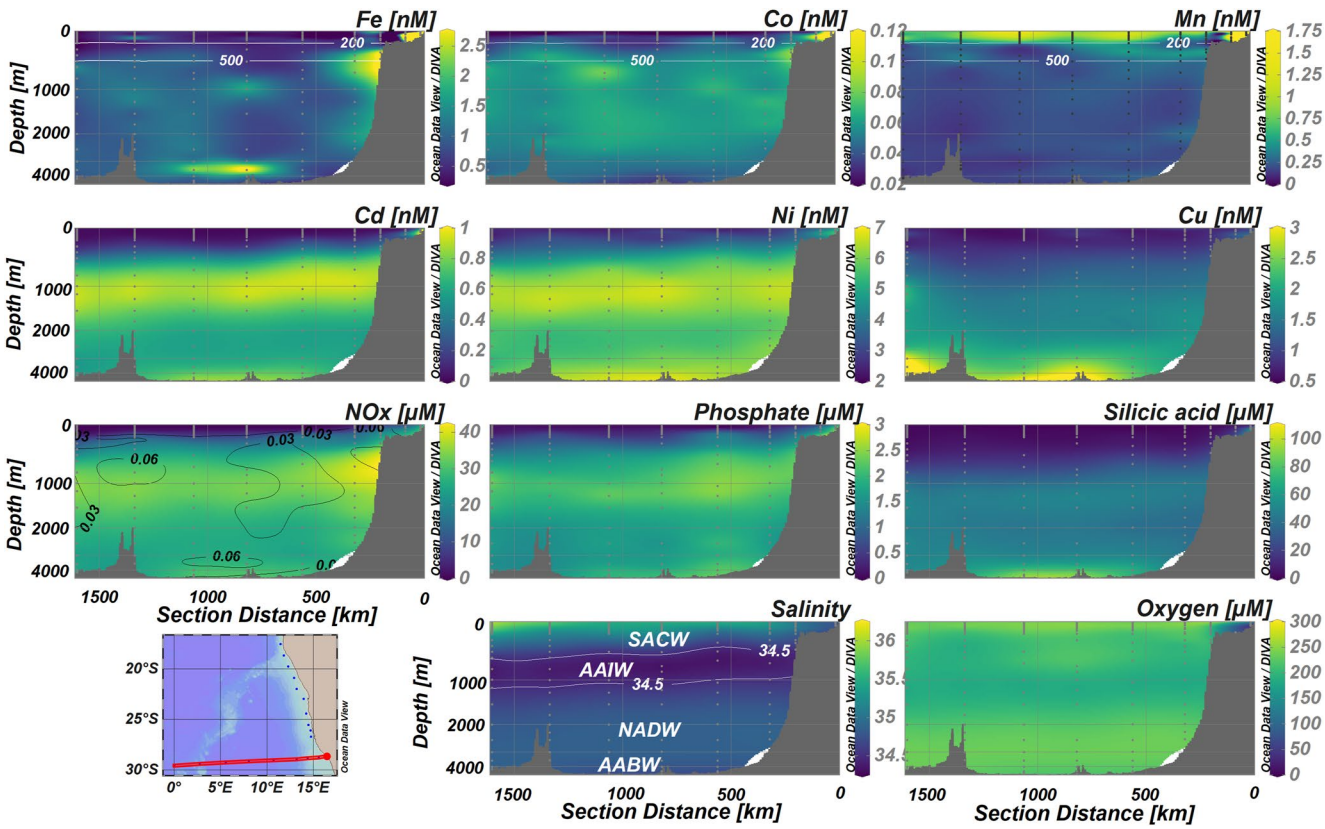


**Figure 3.** Zonal transect along 29°S section plots of dissolved trace metals, $NO_x$ (nitrate + nitrite), oxygen, silicic acid, phosphate and salinity in the Benguela Upwelling System from GA08. Main water masses are indicated in the salinity panel (Liu & Tanhua, 2021). SACW: South Atlantic Central Water, AAIW: Antarctic Intermediate Water, NADW: North Atlantic Deep Water, AABW: Antarctic Bottom Water. Numbers on the top are station numbers. The white horizontal lines on the Fe, Co and Mn panels denote 200 and 500 m depth. Black contour lines in the $NO_x$ panel represent Fe:$NO_x$ = 0.03 and 0.06 nmol µmol$^{-1}$. Figures were produced by Ocean Data View (Schlitzer, 2020).

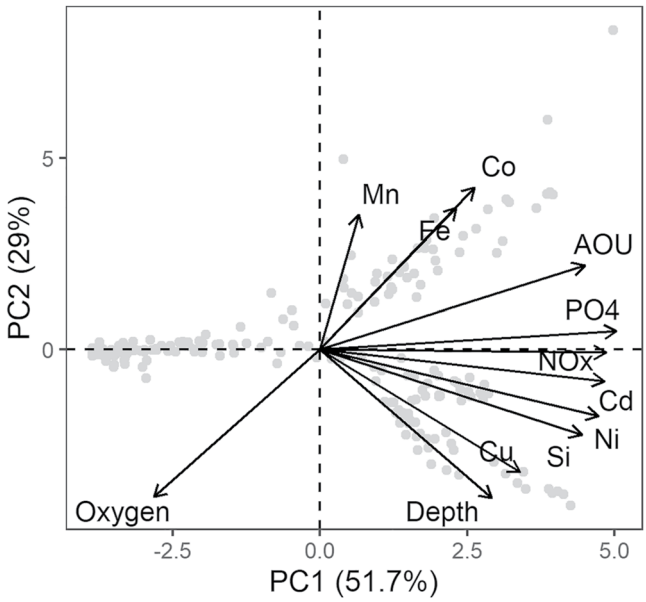


**Figure 4.** Principal component analysis of the M121 Benguela Upwelling System data set. Principal component loadings for each variable are indicated by black vectors. Data points are shown by gray circles.

(Sanial et al., 2018). Subsurface waters with elevated Fe, Co, Mn, and $NO_x$ concentrations extended into the open ocean from the shelf edge at a depth of ~500 m (Figure 3). This plume was less noticeable for Mn, in agreement with observed subsurface Fe, Co, and Mn plumes at ~15°S in the South Atlantic Ocean (Noble et al., 2012). This could be the results of inhibited Mn-oxide dissolution under dark conditions (Sunda et al., 1983) and/or a relative slower scavenging of organically complexed Fe and Co compared to Mn (Parker et al., 2007) along the oxic and organic-rich Namibian shelf edge (Noble et al., 2012). Deeper in the water column, an Fe plume at ~2,000 m was observed (Figure 3), which is remarkably similar to an Fe slope plume observed in the eastern tropical South Pacific suggesting a similar mechanistic origin (John et al., 2018; Lam et al., 2020).

The overall offshore profile distributions of Fe, Co, Cd, Ni, Cu and macronutrients showed depleted surface ocean concentrations with an increase with depth. This reflects uptake in surface waters by microbial organisms and deep water remineralization of sinking/suspended biogenic particles (Bruland et al., 2014; Martin & Michael Gordon, 1988; Yee & Morel, 1996). Depth distributions of Cd and Ni at offshore stations showed strong similarities to those of phosphate, in agreement with other observations (Middag et al., 2018, 2020). Enhanced $NO_x$, phosphate, Cd and Ni concentrations were observed in the water masses of Antarctic Intermediate Water (AAIW) and Antarctic Bottom Water (AABW) relative to North Atlantic Deep Water (NADW), which is in agreement with general observations in the Atlantic Ocean (Middag et al., 2018, 2020). Silicic acid and Cu were mainly enriched in the deep and bottom water masses of NADW and AABW. This behavior of Cu was also observed in the North Atlantic and the North Pacific Ocean (Bruland & Franks, 1983; Roshan & Wu, 2015b). Dissolved Cu concentration in the AABW along our transect were ~2.91 nM (Figure 3), similar to concentrations (~3 nM dCu) reported for the Southern Ocean (Heller & Croot, 2015).

### 4.2. Controlling Factors for Trace Metals in the Benguela Upwelling System

Various processes govern dissolved TM distributions in the BUS. We conducted a Principal Component Analysis (PCA) using the program R for the full BUS data set to assess controlling factors of dissolved TM behavior and distribution in our study area (Figure 4, Table S3 in Supporting Information S1). Two principal components were clearly elucidated. The first principal component (PC1) explains 51.7% of the variance and represents depth and Apparent Oxygen Utilization ($AOU = O_{2\ saturation} - O_{2\ observed}$) dependent variables including Cd, Ni, Cu and macronutrients. Nutrient-type TM distributions for Cd, Ni and Cu are similar to those of macronutrients and controlled by biological uptake in surface water and organic matter remineralization at depth. This is indicated by the positive Pearson correlations between Cd, Ni and all macronutrients, and between Cu and silicic acid ($r > 0.8$). Weaker Pearson correlations between Cu and $NO_x$ and phosphate ($r = 0.48$ and $r = 0.47$, respectively) are likely due to more pronounced benthic sources of Cu, and/or reversible-scavenging, both of which would contribute to a closer correlation between Cu and silicic acid than other macronutrients due to the deeper remineralization depth of silicic acid (Roshan & Wu, 2015b) (Table S4 in Supporting Information S1). The second principal component (PC2, 29%) shows a passive association between redox-sensitive TMs (Fe, Co, Mn) and oxygen (Figure 4). Iron, Mn and Co are important micronutrients, but fall off the trajectory of nutrient-type elements as their distributions along our transect are also strongly influenced by water column oxygen levels alongside biological uptake and remineralization. Sediments overlain by low oxygen waters liberate dissolved reductive phase of Fe and Mn into overlying waters, and also release Co absorbed on Mn oxides. This contributes to enhanced benthic fluxes of Fe, Mn, and Co (Plass et al., 2020, 2021; Schroller-Lomnitz et al., 2019; Shaw et al., 1990), explaining the discrepancies between Fe, Co and Mn and the 'classical' nutrient-type TMs observed. The sensitivity of Mn(IV) oxides to photochemical reduction in sunlit surface waters, and the enhanced stability of Mn(II) exposed to sunlight, explains the slight divergence between Fe and Co, and Mn in the PCA.

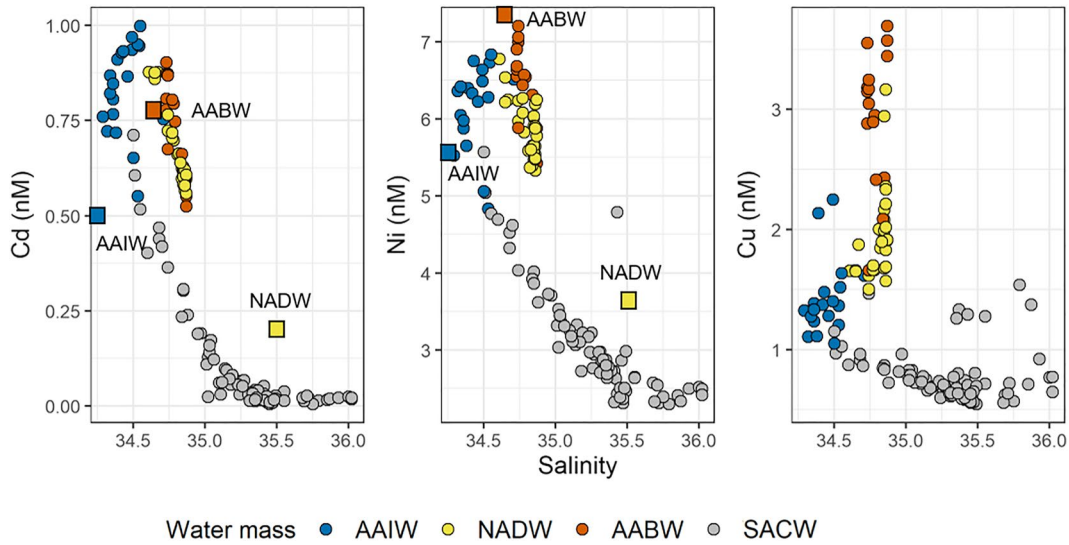


**Figure 5.** Plots of dissolved Cd, Ni, and Cu concentrations against salinity along the ~29°S transect where water masses are subdivided by colors according to neutral density (Liu & Tanhua, 2021). Blue: AAIW (Antarctic Intermediate Water); Yellow: NADW (North Atlantic Deep Water); Orange: AABW (Antarctic Bottom Water); Gray: SACW (South Atlantic Central Water). Colored rectangles are endmember water masses reported in prior works. The physical and chemical properties of the water masses in the eastern South Atlantic have been identified and described in Liu and Tanhua (2021) and are summarized in Table S5 in Supporting Information S1 along with dissolved TM concentrations reported from previous studies (Baars et al., 2014; Boye et al., 2012; Bruland & Franks, 1983; Middag et al., 2018, 2020; Xie et al., 2015, 2019). Endmember concentrations of Cu in these water masses are unavailable to date.

#### 4.2.1. Nutrient-Type Trace Metals—Cd, Ni and Cu

Differences in the concentrations of Cd, Ni and Cu are clear between the AAIW, NADW, and AABW along our ~29°S transect (Figure 5). Intermediate-depth Cd and Ni concentrations ($0.84 \pm 0.12$ nM for Cd and $6.2 \pm 0.5$ nM for Ni) were higher than the average values of AAIW from its source in the Southern Ocean (~0.53 nM for Cd and ~5.59 nM for Ni) (Baars et al., 2014; Boye et al., 2012; Bruland & Franks, 1983; Middag et al., 2018, 2020; Xie et al., 2015, 2019) (Figure 5), probably due to a combination of mixing and accumulation of remineralized Cd and Ni along the northwards transit of AAIW from the Southern Ocean (Roshan & Wu, 2015a). The accumulation of Cu in deep and bottom waters observed along our transect was similar to observations in the North Atlantic and the North Pacific (Bruland & Franks, 1983; Roshan & Wu, 2015b) (Figure 5).

In the OMZ within and outside of the mud belt region (Figure 6, red and blue squares) we observed similar slopes of Ni, Cu, and Cd (not outside mud belt at phosphate >1 μM) versus phosphate compared to ratios in phytoplankton (black dashed lines) (Figure 6) (Ho et al., 2003; C Mark Moore, 2016). This indicates that the supply of phosphate, Ni, Cu and Cd (not outside mud belt at phosphate >1 μM) was determined by the remineralization of sinking phytoplankton debris derived from productive surface waters in the upwelling region. At low phosphate concentrations (phosphate <1 μM) the slopes of Ni, Cu, and Cd versus phosphate at depths >50 m in the open ocean (yellow solid lines) were comparable to those in the mud belt region and phytoplankton ratios (Figure 6). Steeper slopes of Ni, Cu, and Cd versus phosphate were observed in waters with enhanced phosphate concentrations, which can be explained by the Antarctic origin of these waters. Antarctic waters hold enhanced Cd to P (e.g., 0.32–0.36), Ni to P (2.1–2.5) (Middag et al., 2018, 2020) and Cu to P (0.68–1.58) (Hassler & Ellwood, 2019; Janssen et al., 2020; this study) compared to waters with an Atlantic origin. An Antarctic influence on TM to phosphate ratios at enhanced phosphate concentrations is also noticeable in Figure 6. The difference in the slopes of Cd versus phosphate between OMZ stations inside and outside of the mud belt region provides clear evidence against authigenic Cd removal in the upper OMZ water column as proposed in earlier studies (e.g., Conway & John, 2015; Janssen et al., 2014). Bottom dissolved Fe concentrations in the OMZ generally ranged between 5 and 30 nM at the mud belt stations and up to 46 nM outside the mud belt (Figures 2 and 6). The samples with highest phosphate concentrations (Figure 6, highlighted by

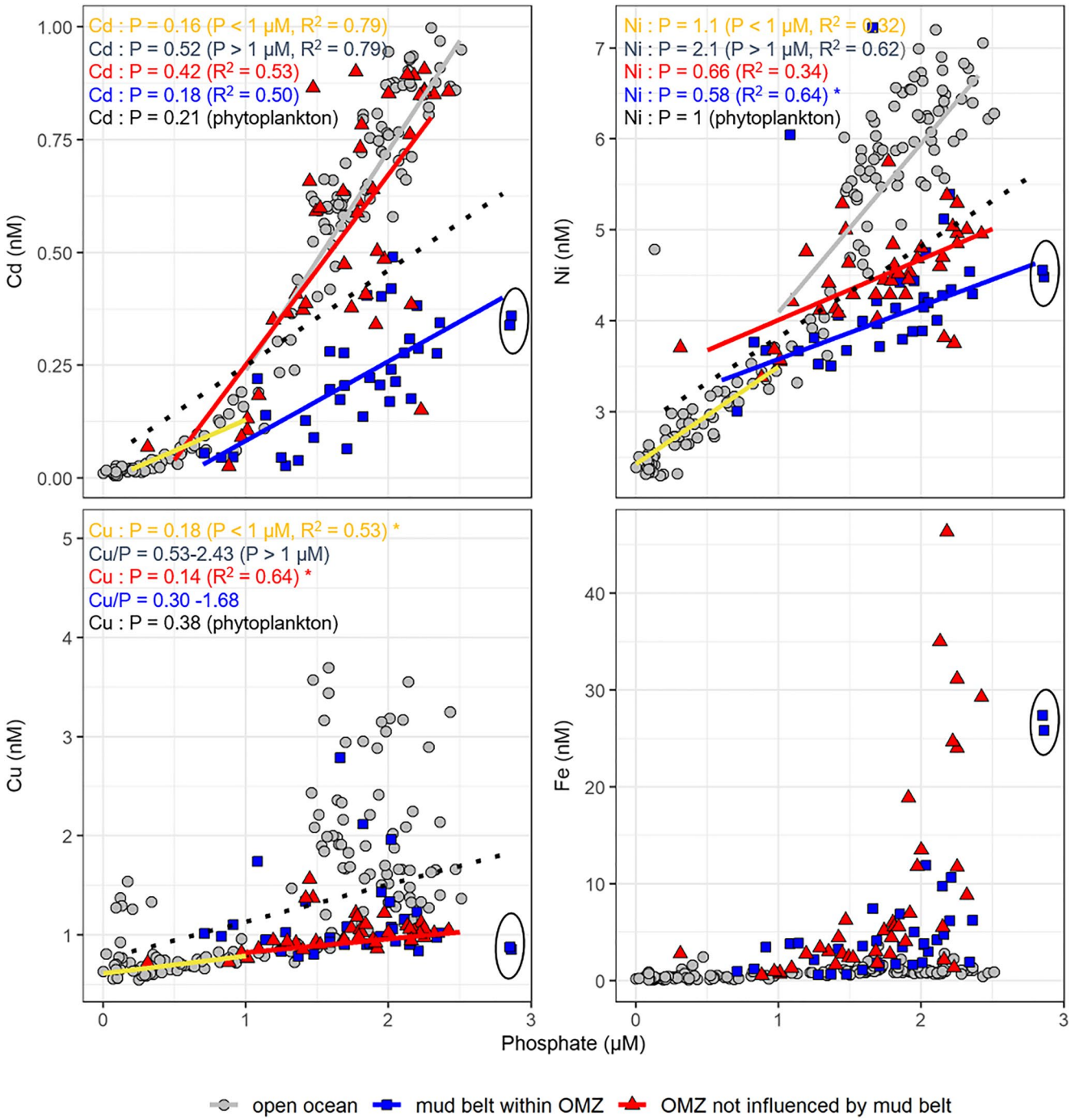


**Figure 6.** Plots of dissolved Cd, Ni, Cu, and Fe against phosphate concentrations at different locations in the Benguela Upwelling System. Locations in open ocean include Stations 35–43. The location of mud belt extends from ~19°S to 24°S with sediment Total Organic Carbon (TOC) >3% and includes Stations 2–4 and Stations 51–52 (Borchers et al., 2005; Bremner, 1980). Stations 44–50 are marked as oxygen minimum zone stations not influenced by the mud belt. Squares within the black oval represent highest phosphate concentrations. Cu/P denotes the spot ratio of Cu to phosphate in different regions, where slopes of Cu versus phosphate show weak correlations ($R^2 < 0.3$). Black dotted lines indicate TM = $(TM/P)_{phytoplankton} \times$ phosphate + $(TM)_{preformed}$, where $(TM/P)_{phytoplankton}$ is from the average TM stoichiometry in phytoplankton (Ho et al., 2003; Moore, 2016) and $(TM)_{preformed}$ is mean TM concentrations in the upper 200 m of the open ocean. * Note datapoints with Ni > 5 nM and Cu > 1 nM were not included in the respective fit.

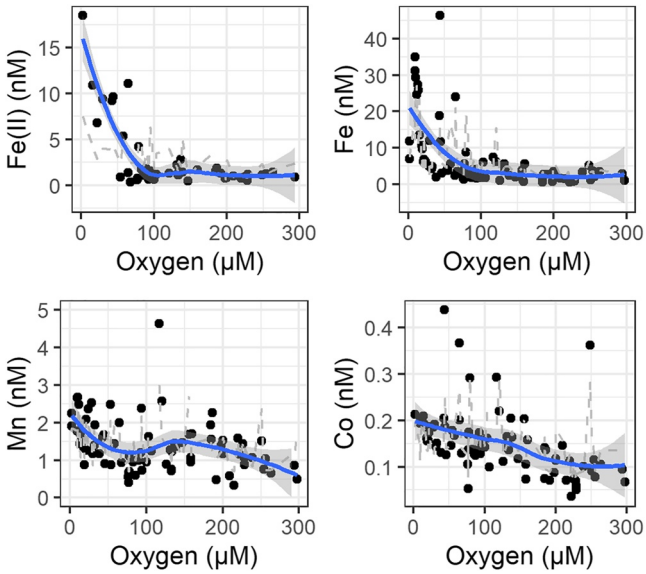


**Figure 7.** Plots of Fe(II), dissolved Fe, Co, Mn against oxygen concentrations for the Namibian shelf. Gray dashed and blue solid lines indicate five point weighted moving average and its smoothed line, respectively, with a gray shaded 95% confidence interval. Note three datapoints with Mn > 5 nM are not shown (but are included in the fit).

black ovals) had moderate Cd, Ni, and Cu concentrations and low oxygen concentrations (~13 μM), with >25 nM Fe (Figures 2 and Figure 6). This implies a pronounced coinciding release of phosphate and Fe in the OMZ by reductive dissolution of iron oxy-hydroxides in sediments, compared to Cd, Ni and Cu (Figure 6 and the following discussions).

### 4.2.2. Redox-Sensitive Trace Metals—Fe, Co and Mn

The co-occurrence of elevated concentrations of Fe, Co, Mn and Fe(II) in suboxic bottom waters on the Namibian shelf (Figure 2), and their close clustering in a PCA analysis, point toward a common source for these redox-sensitive TMs. Enhanced Fe(II) concentrations of >20 nM in bottom waters indicate that reductive dissolution of sedimentary Fe(III) oxy-hydroxides is the mechanism driving enhanced near-bottom Fe concentrations (Noffke et al., 2012; Pakhomova et al., 2007; Plass et al., 2020). Soluble Fe(II) is rapidly oxidized to particulate Fe(III) in the presence of oxygen (Millero et al., 1987), and may also be oxidized under anoxic conditions via coupling to $NO_3^-$ reduction (Scholz et al., 2016). Upon oxidation of dissolved Fe(II) to Fe(III), Fe precipitates lowering dissolved Fe concentrations in the water column (Figure 7). Similarly, slightly increased Mn and Co concentrations in low oxygen waters of the Namibian shelf are likely due to enhanced release from sediments combined with slower oxidations kinetics (Figure 7) (Hawco et al., 2016; Noble et al., 2012).

Concentrations of Fe, Co, Mn and Fe(II) in the water column increased as oxygen levels decreased from 100 μM to <10 μM (Figure 7). Their increase under suboxic conditions (oxygen <100 μM) was highest for Fe(II) followed by Fe and Mn, whilst changes in Co concentration were less noticeable as oxygen levels decreased in the water column (Figure 7). This observation is in line with a study in the same region that demonstrated Mn and Co have a relatively slow oxidation rate under these conditions (Noble et al., 2012). As sedimentary Co delivery is generally associated with Mn-oxides, the impeded oxidation of dissolved Mn under low oxygen conditions is likely a major driver of elevated dissolved Co levels (Heggie & Lewis, 1984). An external shelf source of Fe, Co, and Mn is evidenced by their enhanced concentrations for a given AOU in shelf bottom layer compared with open ocean waters (Figure 8), where relationships between Fe, Co, and Mn and AOU are shaped by physics, remineralization and scavenging (e.g.,

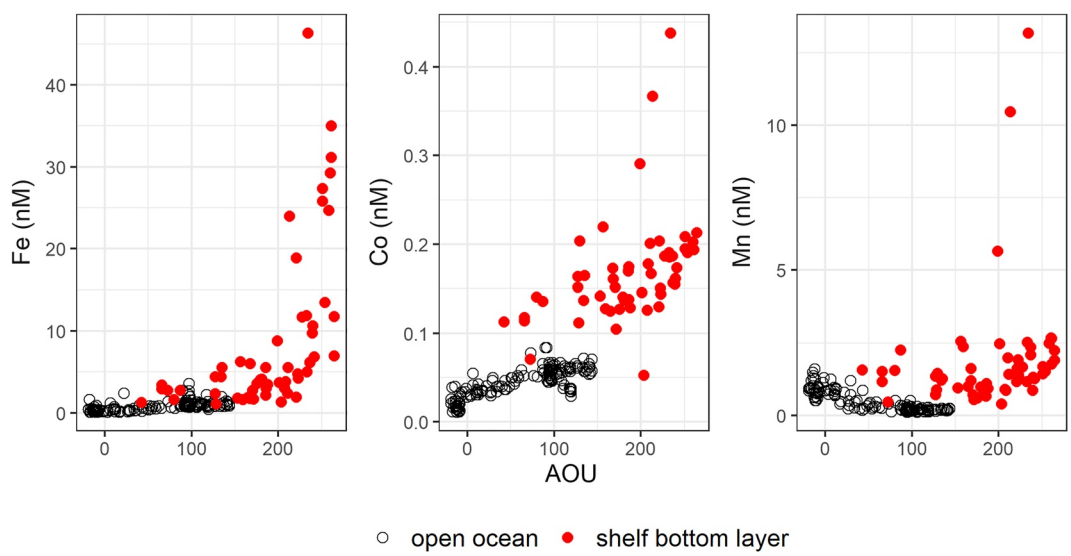


**Figure 8.** Plots of dissolved Fe, Co, and Mn concentrations against apparent oxygen utilization. Open circles are all data points in the open ocean. Red circles are data points deeper than the 26.5 kg $m^{-3}$ isopycnal (the shelf bottom layer) on the Namibian shelf.

Tagliabue et al., 2019). Collectively, all lines of observations provide strong evidence of shelf sedimentary supply of Fe, Co and Mn, where suboxic/anoxic environments facilitate the release of these redox-sensitive TMs from shelf sediments into the overlying waters.

### 4.3. Supply of Sediment-Derived Trace Metals to Shelf Surface Waters and the Open Ocean

#### 4.3.1. Vertical Fluxes of Sediment-Derived Fe, Co, and Mn to Surface Waters on the Shelf

Coastal regions of the BUS are highly productive and no experimental evidence of micro(nutrient) limitation was detected along our shelf cruise section indicating nutrient-replete conditions for primary producers (Browning et al., 2017). However, dissolved Fe, Co, and Mn are deficient relative to macronutrients in the offshore upwelled subsurface waters (e.g., Fe:$N$ = 0.02–0.07 nmol μmol$^{-1}$, Figure 3). Consequently, supplies of TMs such as atmospheric deposition (Jickells et al., 2005; Ventura et al., 2021) and shelf sediments (Johnson et al., 1999) are critical to sustaining high levels of primary productivity on the shelf. We first constrain the vertical fluxes of sediment-derived TMs to shelf surface waters and compare our estimated vertical sediment-derived TM fluxes to those from atmospheric deposition (Barraqueta et al., 2019) in order to determine their relative importance to shelf surface waters.

In general, the net upward supply of Fe, Co, and Mn across the 26.5 kg m$^{-3}$ boundary over the shelf is positive (Table 1), indicating a net TM supply to surface waters from shelf bottom layer. Average vertical Fe and Co fluxes (2.22 ± 0.99 μmol Fe m$^{-2}$ day$^{-1}$ and 0.05 ± 0.03 μmol Co m$^{-2}$ day$^{-1}$) on the Namibian shelf are similar to reported vertical Fe fluxes of 1–2.5 μmol m$^{-2}$ day$^{-1}$ and Co flux of 0.03–0.11 μmol m$^{-2}$ day$^{-1}$ on the Mauritanian shelf with similar seafloor depths (Table 1) (Rapp et al., 2019). Relatively high vertical Fe fluxes were reported for the very inner shelf of Mauritania (13 μmol m$^{-2}$ day$^{-1}$) and Senegal at ∼12°N (16 μmol m$^{-2}$ day$^{-1}$) (Milne et al., 2017; Rapp et al., 2019), which are ∼3 times higher than fluxes at our inner shelf stations (Station 45 and 47, 4.7 ± 1.4 μmol m$^{-2}$ day$^{-1}$ and 4.1 ± 1.9 μmol m$^{-2}$ day$^{-1}$, respectively, Table S6 in Supporting Information S1). A fraction of TMs reaching surface waters will be transported offshore (De Jong et al., 2012; Lohan & Bruland, 2008) and alongshore (Freund, 2020). Our estimates show that alongshore TM fluxes to the north are minor (Table 1). Alongshore fluxes of Fe, Co, and Mn are <5% of their respective upward fluxes.

Atmospheric inputs of TMs are relatively small compared to vertical inputs via upwelling and diffusion to the shelf surface waters. An aluminum-derived estimate of aerosol deposition is ∼0.36 g m$^{-2}$ yr$^{-1}$ in coastal region of the BUS for cruise M121 (Barraqueta et al., 2019). To derive the associated TM fluxes, we assume the composition of dust entering the eastern South Atlantic was the same as the upper continental crust average (5 wt% for Fe, 0.1 wt% for Mn, 0.02 wt‰ for Co, Rudnick & Gao, 2014) as TM-to-aluminum ratios in aerosols from the South Atlantic are similar to the ratio in upper continental crust (Baker et al., 2013; Jickells et al., 2016; Shelley et al., 2017). This assumption is an over simplification as the TM composition of aerosols can be highly variable depending on origin, distance to sources and deposition pathways (wet or dry deposition). However, our study area (∼15–29°S, 0–17°E) is dominated by dry-deposition with a mean precipitation rate of ∼0.15 mm day$^{-1}$ during November and December (Figure S1 in Supporting Information S1), which is almost one order of magni-

**Table 1**
*Namibian Shelf Trace Metal (TM) Fluxes (in μmol m$^{-2}$ day$^{-1}$)*

| | Zonal | | | | | |
|---|---|---|---|---|---|---|
| TMs | Shelf-to-shelf edge | Shelf edge-to-open ocean | Shelf edge-to-open ocean[b] | Upward | Alongshore | Atmospheric deposition[a] |
| Fe | 1.47 ± 0.94 | 0.29 ± 0.20 | 1.02 ± 0.42 | 2.22 ± 0.99 | 0.04 | 0.06 |
| Co | 0.03 ± 0.02 | 0.006 ± 0.004 | 0.03 ± 0.02 | 0.05 ± 0.03 | 0.002 | 2.1 × 10$^{-6}$ |
| Mn | 2.06 ± 1.31 | 0.48 ± 0.31 | – | 0.28 ± 0.11 | 0.01 | 0.004 |

*Note.* Zonal fluxes represent off-shelf fluxes including shelf-to-shelf edge (<500 km from coast) and shelf edge-to-open ocean (500–1,600 km from coast) in the surface layer. Upward fluxes represent fluxes from bottom to surface waters and alongshore fluxes represent equatorward fluxes along the African coast.

[a]Atmospheric TM fluxes to the coastal region of Benguela Upwelling System estimated by dust deposition fluxes in Barraqueta et al. (2019). [b]Shelf edge-to-open ocean are TM fluxes within upper 500 m depth interval.

tude lower than that reported for the region between ~35 and 40°S (Chance et al., 2015). Aerosol trace metal solubility is similarly dependent on multiple factors and varies regionally and temporally. Here we use 7% for Fe, 20% for Mn, and 0.15%–0.73% Co as obtained from measurements using aerosols over the eastern South Atlantic (Chance et al., 2015). Our derived aerosol TM fluxes are thereby 0.06 μmol Fe $m^{-2}$ $day^{-1}$, 0.004 μmol Mn $m^{-2}$ $day^{-1}$ and 2.1 × $10^{-6}$ μmol Co $m^{-2}$ $day^{-1}$ in the shelf surface water, respectively, which are within the range of previous dry-deposition estimates of Fe, Co and Mn between ~35 and 40°S (~0.002–0.135 μmol Fe $m^{-2}$ $day^{-1}$, 0.0001–0.009 μmol Mn $m^{-2}$ $day^{-1}$ and 3–1,400 × $10^{-6}$ μmol Co $m^{-2}$ $day^{-1}$) (Chance et al., 2015). The relatively lower estimated Co deposition fluxes in our study could be the results of the lower abundance of Co in the upper continental crust (~0.02 wt‰) we used here compared with in the anthropogenic-derived dust like coal ash (~0.2 wt‰) (Rudnick & Gao, 2014; Thuróczy et al., 2010). Nevertheless, the atmospheric deposition fluxes of Fe, Co, and Mn are still 1–4 magnitudes lower than their estimated upward fluxes from bottom waters (Table 1). In summary, input of sediment-derived TMs from the shelf bottom layer is the dominant source of TMs to shelf surface waters in the BUS.

#### 4.3.2. Shelf Release as a Major Source of Fe, Co, and Mn to the Eastern South Atlantic

Continental margins act as distinct sources for most TMs to the ocean (Lam & Bishop, 2008; Milne et al., 2017). In the BUS, the overall offshore current in the surface layer can transport TMs from the shelf to the open eastern South Atlantic. To assess the significance of shelf TMs release, we split the 29°S transect into three zones: shelf (on-shelf stations 44–45), shelf edge (on-slope stations 42–43) and open ocean (Stations 35–39) and determine TM fluxes from shelf to shelf edge and shelf edge to open ocean in the surface layer (Table 1). We also calculated shelf edge-to-open ocean TM fluxes for two depth intervals, shallower than the 26.5 kg $m^{-3}$ isopycnal (~200 m) and for the upper 500 m, respectively.

Our estimated Co flux from shelf edge to open ocean (0.03 μmol $m^{-2}$ $day^{-1}$, upper 500 m) is in good agreement with the flux calculated at the shelf edge near Cape Town (0.03 μmol $m^{-2}$ $day^{-1}$, Table 2) using a similar method (Bown et al., 2011). Despite different depth intervals and calculation approaches, our estimated off-shelf Fe flux in the upper 500 m (1.02 μmol $m^{-2}$ $day^{-1}$) is within the range of estimates from other continental shelves (0.02–4 μmol $m^{-2}$ $day^{-1}$, Charette et al., 2016; Hsieh et al., 2021; Milne et al., 2017; Sanial et al., 2018) (Table 2). However, Fe and Co fluxes from the Namibian shelf (1.02 μmol Fe $m^{-2}$ $day^{-1}$ and 0.03 μmol Co $m^{-2}$ $day^{-1}$) are lower than those from the Peruvian shelf into the South Pacific (Table 2, 4 μmol Fe $m^{-2}$ $day^{-1}$ and 0.28 μmol Co $m^{-2}$ $day^{-1}$) (Sanial et al., 2018), likely because the OMZ off the Namibian shelf is weaker than the OMZ off the Peruvian shelf. The extensive OMZ off the Peruvian shelf has been proposed to amplify Co coastal fluxes and support a pronounced Co plume within the OMZ (Hawco et al., 2016). Similarly, the persistent anoxic concentrations over the Peruvian shelf support an extensive Fe(II) plume off the Peruvian shelf, which was estimated to account for approximately half of its total off-shelf Fe fluxes (Cutter et al., 2018; Sanial et al., 2018).

The off-shelf fluxes of TMs from shelf to shelf edge (1.47 μmol Fe $m^{-2}$ $day^{-1}$, 0.03 μmol Co $m^{-2}$ $day^{-1}$ and 2.06 μmol Mn $m^{-2}$ $day^{-1}$, Table 1), correspond to 60%–70% of the Fe and Co upward fluxes. The Mn lateral off-shelf flux is larger than the corresponding upward flux (Table 1), indicating net Mn(II) production in surface water by photochemistry in combination with enhanced Mn(II) stability (Sunda et al., 1983). With

**Table 2**
*Comparison of Shelf-to-Open Ocean Fe, Co and Mn Fluxes (in μmol $m^{-2}$ $day^{-1}$) Between Studies*

| Region | Location | Method | Depth | Fe | Co | Mn | Reference |
|---|---|---|---|---|---|---|---|
| Namibian shelf | ~29°S | $u$ and $K_x$ derived | 500 m | 1.02 | 0.03 | | This study |
| Western N. Atlantic shelf | 0°–70°N | $^{228}$Ra isotope | 200 m | 0.42 | 0.16 | 0.60 | Charette et al. (2016) |
| Senegal Shelf | ~12°N | $u$ and $K_x$ derived | 500 m | 0.21 | | | Milne et al. (2017) |
| Peruvian shelf | ~12°S | $^{228}$Ra isotope | 200 m | 4.00 | 0.28 | 8.89 | Sanial et al. (2018) |
| Cape Basin shelf | ~40°S | $^{228}$Ra isotope | 150 m | 0.02–0.06 | 0.01 | | Hsieh et al. (2021) |
| near Cape Town | ~35°S | $u$ and $K_x$ derived | SML | | 0.03 | | Bown et al. (2011) |
| Congo River Margin | ~3°S | $^{228}$Ra isotope | 15 m | 20.7 | 0.14 | 9.45 | Vieira et al. (2020) |

*Note.* $^{228}$Ra, u, $K_x$, and SML Represent Radium-228 Isotope, Zonal Velocity, Off-Shelf Diffusive Coefficient and Surface mixed Layer, Respectively. For comparison, Fe and Co fluxes from Hsieh et al. (2021) and Vieira et al. (2020) were normalized to the shelf area.

increasing distance from the coast, the TM fluxes to the open ocean above 200 m decrease to 0.29 μmol Fe $m^{-2}$ $day^{-1}$, 0.006 μmol Co $m^{-2}$ $day^{-1}$ and 0.48 μmol Mn $m^{-2}$ $day^{-1}$, which represent an 80%–90% reduction in the flux compared to that reaching the shelf-edge (Table 1). This is the result of biological uptake and scavenging of Fe (Figure 7) (Boyd & Ellwood, 2010; Noble et al., 2012) in combination with limited upwelling at the shelf edge stations (Table S4 in Supporting Information S1). A similar magnitude of decrease was also observed for Fe fluxes along ~12°N zonal transect in the subtropical North Atlantic off Senegal (Milne et al., 2017). In comparison to upper 500 m off-shelf fluxes of Fe and Co, upper 200 m Fe and Co fluxes from shelf edge to open ocean are only 28% and 20% their fluxes in the upper 500 m (Table 1), respectively, indicating that a much larger fraction of Fe and Co from subsurface waters below 200 m is transferred off shelf. Upwelled Fe is quickly oxidized in the surface waters and then precipitates at the shelf edge, resulting in iron enrichment at the shelf edge below 200 m and higher off-shelf subsurface Fe fluxes compared with those in the upper 200 m.

By combining upward and off-shelf fluxes from the shelf to shelf edge, we can elucidate TM cycling within the nearshore area (Figure 9). Reductively mobilized Fe on the shelf is upwelled to the surface waters and transported within the surface waters to the open ocean. However, a large fraction of the Fe laterally transported within the surface water is scavenged and transferred to particulate phases, settling at shelf edge. Iron enriched in oxic sediments at the shelf edge can potentially be mobilized through non-reductive dissolution (Homoky et al., 2013) and stabilized in solution by organic matter (Gledhill, 2012), and then transferred to the open ocean. Although non-reductive dissolution of Fe cannot be assessed using the data in our study, it has been observed at the shelf edge (~34°S) near our study area (Homoky et al., 2013) and likely contributed to the deep plume of Fe at 2,000 m depth. Our estimated subsurface Fe flux from the shelf edge to open ocean (~0.73 μmol $m^{-2}$ $day^{-1}$, difference between upper 500 m and upper 200 m off-shelf Fe fluxes to open ocean) is similar in magnitude to previously estimated benthic Fe fluxes from 733 to 1,182 m at shelf edge sites (0.11–0.23 μmol $m^{-2}$ $day^{-1}$) via non-reductive

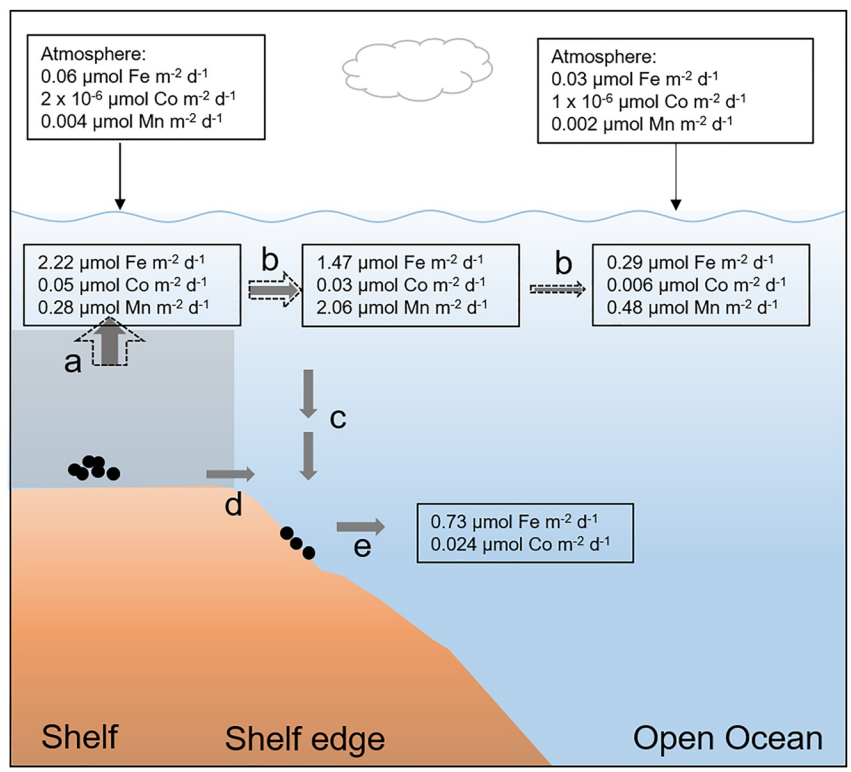


**Figure 9.** Schematic of different trace metal (TM) fluxes in the Benguela Upwelling System. Gray shading indicates oxygen minimum zone over the Namibian shelf. Arrows (a–e) indicate different processes, (a) upward transfer, (b) Lateral off-shelf transfer within the surface layer, (c) precipitation/scavenging to the shelf edge, (d) Lateral transfer within the bottom shelf layer, (e) Off-shelf transfer from the shelf edge. The thickness of arrows (a–c and e) are scaled up to the magnitude of the associated flux. The dashed arrows indicate changes of different TM fluxes following ocean deoxygenation.

**Table 3**
*Sources of Trace Metals to the Eastern South Atlantic From GA08 Cruise*

| TM | Unit | Congo River Margin | Namibian shelf (<500 m) | Namibian shelf (<200 m) | Atmospheric deposition |
|---|---|---|---|---|---|
| Fe | μmol $m^{-2}$ $day^{-1}$ | 20.7 ± 7.00 | 1.02 ± 0.42 | 0.29 ± 0.20 | 0.03 ± 0.03 |
| Co | | 0.14 ± 0.06 | 0.03 ± 0.02 | 0.006 ± 0.004 | $1.0 \pm 1.1 \times 10^{-6}$ |
| Mn | | 9.45 ± 3.65 | | 0.48 ± 0.31 | 0.002 ± 0.002 |
| Fe | mol $yr^{-1}$ | $6.8 \pm 2.3 \times 10^{8}$ | $7.2 \pm 2.9 \times 10^{7}$ | $1.2 \pm 0.8 \times 10^{7}$ | $5.5 \pm 5.5 \times 10^{6}$ |
| Co | | $4.6 \pm 1.8 \times 10^{6}$ | $2.1 \pm 1.4 \times 10^{6}$ | $2.5 \pm 1.6 \times 10^{5}$ | $1.8 \pm 1.8 \times 10^{2}$ |
| Mn | | $3.1 \pm 1.2 \times 10^{8}$ | | $2.0 \pm 1.2 \times 10^{7}$ | $3.6 \pm 3.6 \times 10^{5}$ |

*Note.* For comparison, Fe, Co and Mn fluxes in unit of μmol $m^{-2}$ $day^{-1}$ from Congo River margin (Vieira et al., 2020) were normalized to the shelf area. Atmospheric deposition fluxes of TMs were derived from dust deposition fluxes (0.17 g $m^{-2}$ $yr^{-1}$) in Barraqueta et al. (2019). Namibian shelf areas ($1.1 \times 10^{11}$ $m^2$ and $1.9 \times 10^{11}$ $m^2$ above 200 and 500 m bottom depth respectively) were estimated based on GEBCO's global gridded bathymetric data sets. Surface area of open eastern South Atlantic (17°S–29°S, 0°E–15°E) was $5.0 \times 10^{11}$ $m^2$.

dissolution (Homoky et al., 2013). Stabilization of released Fe by organic ligands is plausibly enhanced at the organic-rich Namibian shelf edge, where >2 wt% Total Organic Carbon (TOC) of sediment surface was observed (Figure 1) (Inthorn et al., 2006). This scenario could partly also explain the cycling of Co. Upwelled Co may not be readily removed via oxidation in shelf waters due to a slow oxidation rates of Co in the water column (Figure 7) (Noble et al., 2012). However, precipitating solid-phase Fe and Mn can remove Co from the water column. In addition, it is possible that lateral transfer of Co within the shelf bottom layer is facilitated by complexation with organic ligands, including siderophores, at the shelf edge (Saito et al., 2005). This Co complexation is reported to have supported >75% total cobalt subsurface plume to the eastern South Atlantic (Noble et al., 2012).

In summary, atmospheric dry depositional TM fluxes are lower than benthic inputs to shelf surface waters and insignificant for Fe, Co and Mn to the open eastern South Atlantic (Table 3). The aerosol deposition flux over the open eastern South Atlantic (17°S–29°S and 0°E–10°E) obtained on the same cruise is estimated at ~0.17 g $m^{-2}$ $yr^{-1}$ based on surface water aluminum concentrations (Barraqueta et al., 2019). Using the same approach and assumptions regarding aerosol composition and TMs solubility described in Section 4.3.1, derived aerosol Fe deposition fluxes are 0.03 μmol Fe $m^{-2}$ $day^{-1}$, $1.0 \times 10^{-6}$ μmol Co $m^{-2}$ $day^{-1}$ and 0.002 μmol Mn $m^{-2}$ $day^{-1}$to the open eastern South Atlantic, which are all slightly lower than our estimates to the shelf sea and within the range of estimates from Chance et al., 2015 further south of our study area. Our estimated atmospheric Fe, Co and Mn fluxes are at least one order of magnitude lower than the corresponding lateral fluxes off the Namibian shelf (Table 3). This indicates that the Namibian shelf is a dominant source of Fe, Co and Mn for the open eastern South Atlantic. In comparison, a previous study has reported much higher TM fluxes to the further north in the eastern South Atlantic from the Congo River (Vieira et al., 2020), which were 1–2 magnitudes higher than the inputs from the Namibian shelf in our study (Table 2) with a far more extensive off-shelf plume. Whilst TMs fluxes from sediments along the BUS are therefore large in a global context, and similar to those derived in other OMZ regions, Fe fluxes are dwarfed by fluxes associated with the offshore advection of the Congo plume.

### 4.4. Global Implications

Shelf sediments are an important source of dissolved Fe to the coastal and open ocean (e.g., Elrod et al., 2004). However, only a small fraction of the shelf sedimentary Fe input is transferred to surface waters on the shelf and exported to the open ocean. The upward Fe fluxes from the bottom to surface waters on the shelf derived in our study (2.22 ± 0.99 μmol $m^{-2}$ $day^{-1}$) and scaled to the Namibian shelf area ($1.1 \times 10^{11}$ $m^2$) amount to $8.9 \pm 4.0 \times 10^{7}$ mol $yr^{-1}$, which is 0.1%–0.5% of the global sedimentary Fe supply in shelf seas of 2.7–8.9 × $10^{10}$ mol $yr^{-1}$ (Dale et al., 2015; Elrod et al., 2004; Tagliabue et al., 2014). Dissolved Fe fluxes from the Namibian shelf to the ocean (Table 3) would account for approximately 0.2%–2.7% of global sedimentary Fe supply in shelf seas if assuming a removal rate of 50%–90% for Fe transported from the shelf to the open ocean (Siedlecki et al., 2012).

Trace metal inputs to shelf waters and the eastern South Atlantic Ocean within our study area are projected to change due to intensifying ocean deoxygenation induced by climate change (Figure 9) (Keeling et al., 2010). Ocean deoxygenation would generate an enhanced benthic Fe, Co, Mn supply on the Namibian shelf. In combination with increased upwelling in the BUS (Lima et al., 2019; Pardo et al., 2011), offshore transport of these shelf-derived TMs from surface or subsurface will alleviate Fe/Co-(co)-limitation of primary production in the eastern South Atlantic (Browning et al., 2017; Siedlecki et al., 2012). If primary productivity increased, intensified remineralization would consume more oxygen and potentially create a positive feedback loop to ocean deoxygenation. The positive feedback loop would continue until $NO_x$ losses due anammox and denitrification in subsurface waters depleted available N stocks. The offshore region would thus potentially become fixed N limited (Wallmann et al., 2022). The biological significance of increasing Fe and Co fluxes off-shelf may therefore be strongly dependent on the response of the N-cycle to intensification of deoxygenation. In any case, Fe/Co/Mn:N ratios are expected to increase following intensification of the shelf OMZ.

## 5. Conclusions

This study shows contrasting distributions of nutrient-type (Cd, Ni, and Cu) and redox-sensitive TMs (Fe, Co, and Mn) in the BUS of the eastern South Atlantic. The reducing sediments on the Namibian shelf contribute redox-sensitive TMs into the overlying water column. Remineralization of sinking phytoplankton debris shapes distributions of Cd, Ni, Cu, and phosphate on the shelf. Atmospheric inputs are often considered as an important source of TMs to the surface ocean (Jickells et al., 2005; Ventura et al., 2021). However, we show shelf sediments off Namibia supply high Fe, Co, and Mn fluxes to both shelf surface waters and to the eastern South Atlantic compared with atmospheric deposition. Off-shelf Fe and Co fluxes to the eastern South Atlantic largely occur from oxic sediments at the shelf edge, where organic matter complexation probably facilitates re-mobilization of Fe and Co.

## Conflict of Interest

The authors declare no conflicts of interest relevant to this study.

## Data Availability Statement

All trace metal and nutrient data have been provided to PANGAEA: https://doi.pangaea.de/10.1594/PANGAEA.947275.

**Acknowledgments**
The authors thank Captain Rainer Hammacher, crew, chief scientist Martin Frank and the scientific party of the *RV Meteor* Cruise M121/GEOTRACES GA08 section. We are grateful for the help from Jaw Chuen Yong, Joaquin Pampin Baro and Christian Schlosser for sample collection; Tim Steffens, Dominik Jasinski and André Mutzberg for technical laboratory assistance. Insa Rapp and Zhi Zeng are thanked for useful discussions on flux calculations. Te Liu acknowledges funding from the China Scholarship Council. Stephan Krisch was financed by GEOMAR and the German Research Foundation (DFG award number AC 217/1-1 to E.A.). R.C.X. was funded by a German DFG individual research grant (project number 432469432). The cruise was funded by the German Research Foundation (Grant Number KO-2906/11-1). Open Access funding enabled and organized by Projekt DEAL.

## References

Baars, O., Abouchami, W., Galer, S. J. G., Boye, M., & Croot, P. L. (2014). Dissolved cadmium in the Southern Ocean: Distribution, speciation, and relation to phosphate. *Limnology & Oceanography*, *59*(2), 385–399. https://doi.org/10.4319/lo.2014.59.2.0385

Baker, A. R., Adams, C., Bell, T. G., Jickells, T. D., & Ganzeveld, L. (2013). Estimation of atmospheric nutrient inputs to the Atlantic Ocean from 50°N to 50°S based on large-scale field sampling: Iron and other dust-associated elements. *Global Biogeochemical Cycles*, *27*(3), 755–767. https://doi.org/10.1002/gbc.20062

Baker, A. R., Jickells, T. D., Witt, M., & Linge, K. L. (2006). Trends in the solubility of iron, aluminium, manganese and phosphorus in aerosol collected over the Atlantic Ocean. *Marine Chemistry*, *98*(1), 43–58. https://doi.org/10.1016/j.marchem.2005.06.004

Barraqueta, J. L. M., Klar, J., Gledhill, M., Schlosser, C., Shelley, R., Planquette, H. F., et al. (2019). Atmospheric deposition fluxes over the Atlantic Ocean: A GEOTRACES case study. *Biogeosciences*, *16*(7), 1525–1542. https://doi.org/10.5194/bg-16-1525-2019

Biller, D. V., & Bruland, K. W. (2013). Sources and distributions of Mn, Fe, Co, Ni, Cu, Zn, and Cd relative to macronutrients along the central California coast during the spring and summer upwelling season. *Marine Chemistry*, *155*, 50–70. https://doi.org/10.1016/j.marchem.2013.06.003

Borchers, S. L., Schnetger, B., Böning, P., & Brumsack, H. J. (2005). Geochemical signatures of the Namibian diatom belt: Perennial upwelling and intermittent anoxia. *Geochemistry, Geophysics, Geosystems*, *6*(6), Q06006. https://doi.org/10.1029/2004GC000886

Bordbar, M. H., Mohrholz, V., & Schmidt, M. (2021). The relation of wind-driven coastal and offshore upwelling in the Benguela Upwelling System. *Journal of Physical Oceanography*, *51*(10), 3117–3133. https://doi.org/10.1175/JPO-D-20-0297.1

Bown, J., Boye, M., Baker, A., Duvieilbourg, E., Lacan, F., Le Moigne, F., et al. (2011). The biogeochemical cycle of dissolved cobalt in the Atlantic and the Southern Ocean south off the coast of South Africa. *Marine Chemistry*, *126*(1–4), 193–206. https://doi.org/10.1016/j.marchem.2011.03.008

Boyd, P. W., & Ellwood, M. J. (2010). The biogeochemical cycle of iron in the ocean. *Nature Geoscience*, *3*(10), 675–682. https://doi.org/10.1038/ngeo964

Boye, M., Wake, B. D., Lopez Garcia, P., Bown, J., Baker, A. R., & Achterberg, E. P. (2012). Distributions of dissolved trace metals (Cd, Cu, Mn, Pb, Ag) in the southeastern Atlantic and the Southern Ocean. *Biogeosciences*, *9*(8), 3231–3246. https://doi.org/10.5194/bg-9-3231-2012

Bremner, J. M. (1980). Physical parameters of the diatomaceous mud belt off South West Africa. *Marine Geology*, *34*(3–4), 67–76. https://doi.org/10.1016/0025-3227(80)90064-X

Browning, T. J., Achterberg, E. P., Engel, A., & Mawji, E. (2021). Manganese co-limitation of phytoplankton growth and major nutrient drawdown in the Southern Ocean. *Nature Communications*, *12*(1), 884. https://doi.org/10.1038/s41467-021-21122-6

Browning, T. J., Achterberg, E. P., Rapp, I., Engel, A., Bertrand, E. M., Tagliabue, A., & Moore, C. M. (2017). Nutrient co-limitation at the boundary of an oceanic gyre. *Nature*, *551*(7679), 242–246. https://doi.org/10.1038/nature24063

Browning, T. J., Rapp, I., Schlosser, C., Gledhill, M., Achterberg, E. P., Bracher, A., & Le Moigne, F. A. C. (2018). Influence of iron, cobalt, and Vitamin $B_{12}$ supply on phytoplankton growth in the tropical East Pacific during the 2015 El Niño. *Geophysical Research Letters*, *45*(12), 6150–6159. https://doi.org/10.1029/2018GL077972

Bruland, K. W., & Franks, R. P. (1983). Mn, Ni, Cu, Zn and Cd in the Western North Atlantic. In *Trace metals in sea water* (pp. 395–414). Springer US. https://doi.org/10.1007/978-1-4757-6864-0_23

Bruland, K. W., Middag, R., & Lohan, M. C. (2014). Controls of trace metals in seawater. In *Treatise on geochemistry*, 2nd ed. (Vol. 8, pp. 19–51). Elsevier. https://doi.org/10.1016/B978-0-08-095975-7.00602-1

Bruland, K. W., Rue, E. L., Smith, G. J., & DiTullio, G. R. (2005). Iron, macronutrients and diatom blooms in the Peru upwelling regime: Brown and blue waters of Peru. *Marine Chemistry*, *93*(2–4), 81–103. https://doi.org/10.1016/j.marchem.2004.06.011

Carr, M.-E. (2001). Estimation of potential productivity in Eastern Boundary Currents using remote sensing. *Deep Sea Research Part II: Topical Studies in Oceanography*, *49*(1–3), 59–80. https://doi.org/10.1016/S0967-0645(01)00094-7

Chance, R., Jickells, T. D., & Baker, A. R. (2015). Atmospheric trace metal concentrations, solubility and deposition fluxes in remote marine air over the south-east Atlantic. *Marine Chemistry*, *177*, 45–56. https://doi.org/10.1016/j.marchem.2015.06.028

Charette, M. A., Lam, P. J., Lohan, M. C., Kwon, E. Y., Hatje, V., Jeandel, C., et al. (2016). Coastal ocean and shelf-sea biogeochemical cycling of trace elements and isotopes: Lessons learned from GEOTRACES. *Philosophical Transactions of the Royal Society A: Mathematical, Physical & Engineering Sciences*, *374*(2081), 20160076. https://doi.org/10.1098/rsta.2016.0076

Chavez, F. P., & Messié, M. (2009). A comparison of Eastern boundary upwelling ecosystems. *Progress in Oceanography*, *83*(1–4), 80–96. https://doi.org/10.1016/j.pocean.2009.07.032

Chelton, D. B., DeSzoeke, R. A., Schlax, M. G., El Naggar, K., Siwertz, N., & Nicolas, S. (1998). Geographical variability of the first baroclinic Rossby radius of deformation. *Journal of Physical Oceanography*, *28*(3), 433–460. https://doi.org/10.1175/1520-0485(1998)028%3C0433:GVOTFB%3E2.0.CO;2

Conway, T. M., & John, S. G. (2015). The cycling of iron, zinc and cadmium in the North East Pacific Ocean—Insights from stable isotopes. *Geochimica et Cosmochimica Acta*, *164*, 262–283. https://doi.org/10.1016/j.gca.2015.05.023

Croot, P. L., & Laan, P. (2002). Continuous shipboard determination of Fe(II) in polar waters using flow injection analysis with chemiluminescence detection. *Analytica Chimica Acta*, *466*(2), 261–273. https://doi.org/10.1016/S0003-2670(02)00596-2

Curl, H., & Hill, M. N. (1964). Progress in the study of the Seas. The sea: Ideas and observations on progress in the study of the seas. *Ecology*, *45*(3), 664. https://doi.org/10.2307/1936129

Cutter, G., Casciotti, K., Croot, P., Geibert, W., Heimbürger, L.-E., Lohan, M., et al. (2017). Sampling and Sample-handling Protocols for GEOTRACES Cruises. Version 3, August 2017. Retrieved from http://www.geotraces.org/sic/intercalibrate-data/cookbook

Cutter, G., Moffett, J. W., Nielsdóttir, M. C., & Sanial, V. (2018). Multiple oxidation state trace elements in suboxic waters off Peru: In situ redox processes and advective/diffusive horizontal transport. *Marine Chemistry*, *201*, 77–89. https://doi.org/10.1016/j.marchem.2018.01.003

Dale, A. W., Nickelsen, L., Scholz, F., Hensen, C., Oschlies, A., & Wallmann, K. (2015). A revised global estimate of dissolved iron fluxes from marine sediments. *Global Biogeochemical Cycles*, *29*(5), 691–707. https://doi.org/10.1002/2014GB005017

De Jong, J., Schoemann, V., Lannuzel, D., Croot, P., De Baar, H., & Tison, J. L. (2012). Natural iron fertilization of the Atlantic sector of the Southern Ocean by continental shelf sources of the Antarctic Peninsula. *Journal of Geophysical Research*, *117*(1), GO1029. https://doi.org/10.1029/2011JG001679

Dittmar, T., & Birkicht, M. (2001). Regeneration of nutrients in the northern Benguela upwelling and the Angola-Benguela front areas. *South African Journal of Science*, *97*(5–6), 239–246.

Dunckley, J. F., Koseff, J. R., Steinbuck, J. V., Monismith, S. G., & Genin, A. (2012). Comparison of mixing efficiency and vertical diffusivity models from temperature microstructure. *Journal of Geophysical Research*, *117*(C10), 10008. https://doi.org/10.1029/2012JC007967

Elrod, V. A., Berelson, W. M., Coale, K. H., & Johnson, K. S. (2004). The flux of iron from continental shelf sediments: A missing source for global budgets. *Geophysical Research Letters*, *31*(12), 2–5. https://doi.org/10.1029/2004GL020216

Fairall, C. W., Bradley, E. F., Hare, J. E., Grachev, A. A., & Edson, J. B. (2003). Bulk parameterization of air–sea fluxes: Updates and verification for the COARE algorithm. *Journal of Climate*, *16*(4), 571–591. https://doi.org/10.1175/1520-0442(2003)016<0571:bpoasf>2.0.co;2

Flynn, R. F., Granger, J., Veitch, J. A., Siedlecki, S., Burger, J. M., Pillay, K., & Fawcett, S. E. (2020). On-shelf nutrient trapping enhances the fertility of the southern Benguela upwelling system. *Journal of Geophysical Research: Oceans*, *125*(6), 1–24. https://doi.org/10.1029/2019JC015948

Freund, M. (2020). Dispersion of a tracer in the eastern tropical South Pacific—An investigation of interactions from the benthic boundary layer to the ocean interior. Doctoral dissertation. Retrieved from https://nbn-resolving.org/urn:nbn:de:gbv:8-mods-2020-00162-9

Garzoli, S. L., & Gordon, A. L. (1996). Origins and variability of the Benguela current. *Journal of Geophysical Research*, *101*(C1), 897–906. https://doi.org/10.1029/95JC03221

Gill, A. E., & Adrian, E. (1982). *Atmosphere-ocean dynamics* (Vol. 30). Academic press.

Gledhill, M. (2012). The organic complexation of iron in the marine environment: A review. *Frontiers in Microbiology*, *3*, 1–17. https://doi.org/10.3389/fmicb.2012.00069

Glover, D. M., Jenkins, W. J., & Doney, S. C. (2011). *Modeling methods for marine science*. Cambridge University Press. https://doi.org/10.1017/CBO9780511975721

Grasshoff, K., Kremling, K., & Ehrhardt, M. (1999). Methods of seawater analysis. In K. Grasshoff, K. Kremling, & M. Ehrhardt (Eds.), *Methods of seawater analysis: Third, completely revised and extended edition*. Wiley. https://doi.org/10.1002/9783527613984

Hassler, C., & Ellwood, M. (2019). Nutrient concentration in seawater samples, collected from the underway supply, CTD and trace metal rosettes in the Southern Ocean during the austral summer of 2016/2017, on board the Antarctic Circumnavigation Expedition (ACE). https://doi.org/10.5281/ZENODO.2616606

Hawco, N. J., Ohnemus, D. C., Resing, J. A., Twining, B. S., & Saito, M. A. (2016). A dissolved cobalt plume in the oxygen minimum zone of the eastern tropical South Pacific. *Biogeosciences*, *13*(20), 5697–5717. https://doi.org/10.5194/bg-13-5697-2016

Heggie, D., & Lewis, T. (1984). Cobalt in pore waters of marine sediments. *Nature*, *311*(5985), 453–455. https://doi.org/10.1038/311453a0

Heller, M. I., & Croot, P. L. (2015). Copper speciation and distribution in the Atlantic sector of the Southern Ocean. *Marine Chemistry*, *173*, 253–268. https://doi.org/10.1016/j.marchem.2014.09.017

Ho, T. Y., Quigg, A., Finkel, Z. V., Milligan, A. J., Wyman, K., Falkowski, P. G., & Morel, F. M. M. (2003). The elemental composition of some marine phytoplankton. *Journal of Phycology*, *39*(6), 1145–1159. https://doi.org/10.1111/j.0022-3646.2003.03-090.x

Homoky, W. B., John, S. G., Conway, T. M., & Mills, R. A. (2013). Distinct iron isotopic signatures and supply from marine sediment dissolution. *Nature Communications*, *4*(1), 2143. https://doi.org/10.1038/ncomms3143

Homoky, W. B., Severmann, S., McManus, J., Berelson, W. M., Riedel, T. E., Statham, P. J., & Mills, R. A. (2012). Dissolved oxygen and suspended particles regulate the benthic flux of iron from continental margins. *Marine Chemistry*, *134*(135), 59–70. https://doi.org/10.1016/j.marchem.2012.03.003

Hopwood, M. J., Birchill, A. J., Gledhill, M., Achterberg, E. P., Klar, J. K., & Milne, A. (2017). A comparison between four analytical methods for the measurement of Fe(II) at nanomolar concentrations in coastal seawater. *Frontiers in Marine Science*, *4*, 1–14. https://doi.org/10.3389/fmars.2017.00192

Hsieh, Y.-T., Geibert, W., Woodward, E. M. S., Wyatt, N. J., Lohan, M. C., Achterberg, E. P., & Henderson, G. M. (2021). Radium-228-derived ocean mixing and trace element inputs in the South Atlantic. *Biogeosciences*, *18*(5), 1645–1671. https://doi.org/10.5194/bg-18-1645-2021

Hutchings, L., van der Lingen, C. D., Shannon, L. J., Crawford, R. J. M., Verheye, H. M. S., Bartholomae, C. H., et al. (2009). The Benguela Current: An ecosystem of four components. *Progress in Oceanography*, *83*(1–4), 15–32. https://doi.org/10.1016/j.pocean.2009.07.046

Hutchins, D. A., & Bruland, K. W. (1998). Iron-limited diatom growth and Si:N uptake ratios in a coastal upwelling regime. *Nature*, *393*(6685), 561–564. https://doi.org/10.1038/31203

Inthorn, M., Wagner, T., Scheeder, G., & Zabel, M. (2006). Lateral transport controls distribution, quality, and burial of organic matter along continental slopes in high-productivity areas. *Geology*, *34*(3), 205. https://doi.org/10.1130/G22153.1

Janssen, D. J., Conway, T. M., John, S. G., Christian, J. R., Kramer, D. I., Pedersen, T. F., & Cullen, J. T. (2014). Undocumented water column sink for cadmium in open ocean oxygen-deficient zones. *Proceedings of the National Academy of Sciences*, *111*(19), 6888–6893. https://doi.org/10.1073/pnas.1402388111

Janssen, D. J., Sieber, M., Ellwood, M. J., Conway, T. M., Barrett, P. M., Chen, X., et al. (2020). Dissolved trace metal (Fe, Ni, Cu, Zn, Cd, Pb) concentrations in the Indian and Pacific sectors of the Southern Ocean from the Antarctic circumnavigation expedition (2016–2017). https://doi.org/10.5281/ZENODO.3634411

Jarre, A., Hutchings, L., Kirkman, S. P., Kreiner, A., Tchipalanga, P. C. M., Kainge, P., et al. (2015). Synthesis: Climate effects on biodiversity, abundance and distribution of marine organisms in the Benguela. *Fisheries Oceanography*, *24*(S1), 122–149. https://doi.org/10.1111/fog.12086

Jickells, T. (1999). The inputs of dust derived elements to the Sargasso Sea; a synthesis. *Marine Chemistry*, *68*(1–2), 5–14. https://doi.org/10.1016/S0304-4203(99)00061-4

Jickells, T. D., An, Z. S., Andersen, K. K., Baker, A. R., Bergametti, G., Brooks, N., et al. (2005). Global iron connections between desert dust, ocean biogeochemistry, and climate. *Science*, *308*(5718), 67–71. https://doi.org/10.1126/science.1105959

Jickells, T. D., Baker, A. R., & Chance, R. (2016). Atmospheric transport of trace elements and nutrients to the oceans. *Philosophical Transactions of the Royal Society A: Mathematical, Physical & Engineering Sciences*, *374*(2081), 20150286. https://doi.org/10.1098/rsta.2015.0286

John, S. G., Helgoe, J., Townsend, E., Weber, T., DeVries, T., Tagliabue, A., et al. (2018). Biogeochemical cycling of Fe and Fe stable isotopes in the Eastern tropical South Pacific. *Marine Chemistry*, *201*(March), 66–76. https://doi.org/10.1016/j.marchem.2017.06.003

Johnson, K. S., Chavez, F. P., & Friederich, G. E. (1999). Continental-shelf sediment as a primary source of iron for coastal phytoplankton. *Nature*, *398*(6729), 697–700. https://doi.org/10.1038/19511

Johnson, K. S., Gordon, R. M., & Coale, K. H. (1997). What controls dissolved iron concentrations in the world ocean? *Marine Chemistry*, *57*(3–4), 137–161. https://doi.org/10.1016/S0304-4203(97)00043-1

Junker, T., Mohrholz, V., Siegfried, L., & van der Plas, A. (2017). Seasonal to interannual variability of water mass characteristics and currents on the Namibian shelf. *Journal of Marine Systems*, *165*, 36–46. https://doi.org/10.1016/J.JMARSYS.2016.09.003

Karstensen, J., Stramma, L., & Visbeck, M. (2008). Oxygen minimum zones in the eastern tropical Atlantic and Pacific oceans. *Progress in Oceanography*, *77*(4), 331–350. https://doi.org/10.1016/j.pocean.2007.05.009

Keeling, R. F., Körtzinger, A., & Gruber, N. (2010). Ocean deoxygenation in a warming world. *Annual Review of Marine Science*, *2*(1), 199–229. https://doi.org/10.1146/annurev.marine.010908.163855

Lam, P. J., & Bishop, J. K. B. (2008). The continental margin is a key source of iron to the HNLC North Pacific Ocean. *Geophysical Research Letters*, *35*(7), 1–5. https://doi.org/10.1029/2008GL033294

Lam, P. J., Heller, M. I., Lerner, P. E., Moffett, J. W., & Buck, K. N. (2020). Unexpected source and transport of iron from the deep Peru margin. *ACS Earth and Space Chemistry*, *4*(7), 977–992. https://doi.org/10.1021/acsearthspacechem.0c00066

Landolfi, A., Dietze, H., Koeve, W., & Oschlies, A. (2013). Overlooked runaway feedback in the marine nitrogen cycle: The vicious cycle. *Biogeosciences*, *10*(3), 1351–1363. https://doi.org/10.5194/bg-10-1351-2013

Lima, D. C. A., Soares, P. M. M., Semedo, A., Cardoso, R. M., Cabos, W., & Sein, D. V. (2019). How will a warming climate Affect the Benguela coastal low-level wind jet? *Journal of Geophysical Research: Atmospheres*, *124*(9), 5010–5028. https://doi.org/10.1029/2018JD029574

Liu, M., & Tanhua, T. (2021). Water masses in the Atlantic Ocean: Characteristics and distributions. *Ocean Science*, *17*(2), 463–486. https://doi.org/10.5194/os-17-463-2021

Lohan, M. C., & Bruland, K. W. (2008). Elevated Fe(II) and dissolved Fe in hypoxic shelf waters off Oregon and Washington: An enhanced source of iron to coastal upwelling regimes. *Environmental Science and Technology*, *42*(17), 6462–6468. https://doi.org/10.1021/es800144j

Martin, J. H., & Michael Gordon, R. (1988). Northeast Pacific iron distributions in relation to phytoplankton productivity. *Deep-Sea Research, Part A: Oceanographic Research Papers*, *35*(2), 177–196. https://doi.org/10.1016/0198-0149(88)90035-0

Mercier, H., Arhan, M., & Lutjeharms, J. R. E. (2003). Upper-layer circulation in the eastern Equatorial and south Atlantic Ocean in January–March 1995. *Deep Sea Research Part I: Oceanographic Research Papers*, *50*(7), 863–887. https://doi.org/10.1016/S0967-0637(03)00071-2

Middag, R., de Baar, H. J. W., Bruland, K. W., & van Heuven, S. M. A. C. (2020). The distribution of nickel in the west-Atlantic Ocean, its relationship with phosphate and a comparison to cadmium and zinc. *Frontiers in Marine Science*, *7*, 1–17. https://doi.org/10.3389/fmars.2020.00105

Middag, R., van Heuven, S. M. A. C., Bruland, K. W., & de Baar, H. J. W. (2018). The relationship between cadmium and phosphate in the Atlantic Ocean unravelled. *Earth and Planetary Science Letters*, *492*, 79–88. https://doi.org/10.1016/j.epsl.2018.03.046

Millero, F. J., Sotolongo, S., & Izaguirre, M. (1987). The oxidation kinetics of Fe(II) in seawater. *Geochimica et Cosmochimica Acta*, *51*(4), 793–801. https://doi.org/10.1016/0016-7037(87)90093-7

Milne, A., Schlosser, C., Wake, B. D., Achterberg, E. P., Chance, R., Baker, A. R., et al. (2017). Particulate phases are key in controlling dissolved iron concentrations in the (sub)tropical North Atlantic. *Geophysical Research Letters*, *44*(5), 2377–2387. https://doi.org/10.1002/2016GL072314

Mohrholz, V., Bartholomae, C. H., van der Plas, A. K., & Lass, H. U. (2008). The seasonal variability of the northern Benguela undercurrent and its relation to the oxygen budget on the shelf. *Continental Shelf Research*, *28*(3), 424–441. https://doi.org/10.1016/j.csr.2007.10.001

Mohrholz, V., Eggert, A., Junker, T., Nausch, G., Ohde, T., & Schmidt, M. (2014). Cross shelf hydrographic and hydrochemical conditions and their short term variability at the northern Benguela during a normal upwelling season. *Journal of Marine Systems*, *140*(PB), 92–110. https://doi.org/10.1016/J.JMARSYS.2014.04.019

Monteiro, P. M. S., & van der Plas, A. K. (2006). 5 Low oxygen water (LOW) variability in the Benguela system: Key processes and forcing scales relevant to forecasting. *Large Marine Ecosystems*, *14*, 71–90. https://doi.org/10.1016/S1570-0461(06)80010-8

Monterey, G. I., & DeWitt, L. M. (2000). *Seasonal variability of global mixed layer depth from WOD98 temperature and salinity profiles*. NOAA Technical Memorandum NMFS.

Moore, C. M. (2016). Diagnosing oceanic nutrient deficiency. *Philosophical Transactions of the Royal Society A: Mathematical, Physical & Engineering Sciences*, *374*(2081), 20150290. https://doi.org/10.1098/rsta.2015.0290

Moore, C. M., Mills, M. M., Arrigo, K. R., Berman-Frank, I., Bopp, L., Boyd, P. W., et al. (2013). Processes and patterns of oceanic nutrient limitation. *Nature Geoscience*, *6*(9), 701–710. https://doi.org/10.1038/ngeo1765

Nelson, L. V. S., Bay, R., Town, C., Africa, S., Wefer, G., Berger, W. H., et al. (1996). The Benguela: Large scale features and processes and system variability. *The South Atlantic*, 163–210. https://doi.org/10.1007/978-3-642-80353-6_9

Noble, A. E., Lamborg, C. H., Ohnemus, D. C., Lam, P. J., Goepfert, T. J., Measures, C. I., et al. (2012). Basin-scale inputs of cobalt, iron, and manganese from the Benguela-Angola front to the South Atlantic Ocean. *Limnology & Oceanography*, *57*(4), 989–1010. https://doi.org/10.4319/lo.2012.57.4.0989

Noffke, A., Hensen, C., Sommer, S., Scholz, F., Bohlen, L., Mosch, T., et al. (2012). Benthic iron and phosphorus fluxes across the Peruvian oxygen minimum zone. *Limnology & Oceanography*, *57*(3), 851–867. https://doi.org/10.4319/lo.2012.57.3.0851

Okubo, A. (1971). Oceanic diffusion diagrams. *Deep-Sea Research and Oceanographic Abstracts*, *18*(8), 789–802. https://doi.org/10.1016/0011-7471(71)90046-5

Pakhomova, S. V., Hall, P. O. J., Kononets, M. Y., Rozanov, A. G., Tengberg, A., & Vershinin, A. V. (2007). Fluxes of iron and manganese across the sediment-water interface under various redox conditions. *Marine Chemistry*, *107*(3), 319–331. https://doi.org/10.1016/j.marchem.2007.06.001

Pardo, P. C., Padín, X. A., Gilcoto, M., Farina-Busto, L., & Pérez, F. F. (2011). Evolution of upwelling systems coupled to the long-term variability in sea surface temperature and Ekman transport. *Climate Research*, *48*(2–3), 231–246. https://doi.org/10.3354/cr00989

Parker, D. L., Morita, T., Mozafarzadeh, M. L., Verity, R., McCarthy, J. K., & Tebo, B. M. (2007). Inter-relationships of $MnO_2$ precipitation, siderophore–Mn(III) complex formation, siderophore degradation, and iron limitation in Mn(II)-oxidizing bacterial cultures. *Geochimica et Cosmochimica Acta*, *71*(23), 5672–5683. https://doi.org/10.1016/J.GCA.2007.03.042

Peterson, R. G., & Stramma, L. (1991). Upper-level circulation in the south Atlantic Ocean. *Progress in Oceanography*, *26*(1), 1–73. https://doi.org/10.1016/0079-6611(91)90006-8

Plass, A., Dale, A. W., & Scholz, F. (2021). Sedimentary cycling and benthic fluxes of manganese, cobalt, nickel, copper, zinc and cadmium in the Peruvian oxygen minimum zone. *Marine Chemistry*, *233*, 103982. https://doi.org/10.1016/j.marchem.2021.103982

Plass, A., Schlosser, C., Sommer, S., Dale, A. W., Achterberg, E. P., & Scholz, F. (2020). The control of hydrogen sulfide on benthic iron and cadmium fluxes in the oxygen minimum zone off Peru. *Biogeosciences*, *17*(13), 3685–3704. https://doi.org/10.5194/bg-17-3685-2020

Rae, C. D. (2005). A demonstration of the hydrographic partition of the Benguela upwelling ecosystem at 26°40'S. *African Journal of Marine Science*, *27*(3), 617–628. https://doi.org/10.2989/18142320509504122

Rapp, I., Schlosser, C., Browning, T. J., Wolf, F., Le Moigne, F. A. C., Gledhill, M., & Achterberg, E. P. (2020). El Niño-driven oxygenation impacts Peruvian shelf iron supply to the south Pacific ocean. *Geophysical Research Letters*, *47*(7). https://doi.org/10.1029/2019GL086631

Rapp, I., Schlosser, C., Menzel Barraqueta, J.-L., Wenzel, B., Lüdke, J., Scholten, J., et al. (2019). Controls on redox-sensitive trace metals in the Mauritanian oxygen minimum zone. *Biogeosciences*, *16*(21), 4157–4182. https://doi.org/10.5194/bg-16-4157-2019

Rapp, I., Schlosser, C., Rusiecka, D., Gledhill, M., & Achterberg, E. P. (2017). Automated preconcentration of Fe, Zn, Cu, Ni, Cd, Pb, Co, and Mn in seawater with analysis using high-resolution sector field inductively-coupled plasma mass spectrometry. *Analytica Chimica Acta*, *976*, 1–13. https://doi.org/10.1016/j.aca.2017.05.008

Roshan, S., & Wu, J. (2015a). Cadmium regeneration within the north Atlantic. *Global Biogeochemical Cycles*, *29*(12), 2082–2094. https://doi.org/10.1002/2015GB005215

Roshan, S., & Wu, J. (2015b). The distribution of dissolved copper in the tropical-subtropical north Atlantic across the GEOTRACES GA03 transect. *Marine Chemistry*, *176*, 189–198. https://doi.org/10.1016/j.marchem.2015.09.006

Rudnick, R. L., & Gao, S. (2014). Composition of the continental crust. In *Treatise on geochemistry* (Vol. 3, pp. 1–51). Elsevier. https://doi.org/10.1016/B978-0-08-095975-7.00301-6

Saito, M. A., Moffett, J. W., Chisholm, S. W., & Waterbury, J. B. (2002). Cobalt limitation and uptake in Prochlorococcus. *Limnology & Oceanography*, *47*(6), 1629–1636. https://doi.org/10.4319/lo.2002.47.6.1629

Saito, M. A., Rocap, G., & Moffett, J. W. (2005). Production of cobalt binding ligands in a *Synechococcus* feature at the Costa Rica upwelling dome. *Limnology & Oceanography*, *50*(1), 279–290. https://doi.org/10.4319/lo.2005.50.1.0279

Sanial, V., Kipp, L. E., Henderson, P. B., van Beek, P., Reyss, J. L., Hammond, D. E., et al. (2018). Radium-228 as a tracer of dissolved trace element inputs from the Peruvian continental margin. *Marine Chemistry*, *201*, 20–34. https://doi.org/10.1016/j.marchem.2017.05.008

Schlitzer, R. (2020). Ocean Data View. Retrieved from http://odv.awi.de

Scholz, F., Löscher, C. R., Fiskal, A., Sommer, S., Hensen, C., Lomnitz, U., et al. (2016). Nitrate-dependent iron oxidation limits iron transport in anoxic ocean regions. *Earth and Planetary Science Letters*, *454*, 272–281. https://doi.org/10.1016/j.epsl.2016.09.025

Schroller-Lomnitz, U., Hensen, C., Dale, A. W., Scholz, F., Clemens, D., Sommer, S., et al. (2019). Dissolved benthic phosphate, iron and carbon fluxes in the Mauritanian upwelling system and implications for ongoing deoxygenation. *Deep Sea Research Part I: Oceanographic Research Papers*, *143*, 70–84. https://doi.org/10.1016/j.dsr.2018.11.008

Shaw, T. J., Gieskes, J. M., & Jahnke, R. A. (1990). Early diagenesis in differing depositional environments: The response of transition metals in pore water. *Geochimica et Cosmochimica Acta*, *54*(5), 1233–1246. https://doi.org/10.1016/0016-7037(90)90149-F

Shelley, R. U., Roca-Martí, M., Castrillejo, M., Sanial, V., Masqué, P., Landing, W. M., et al. (2017). Quantification of trace element atmospheric deposition fluxes to the Atlantic Ocean (>40°N; GEOVIDE, GEOTRACES GA01) during spring 2014. *Deep Sea Research Part I: Oceanographic Research Papers*, *119*, 34–49. https://doi.org/10.1016/j.dsr.2016.11.010

Shillington, F. A., Reason, C. J. C., Duncombe Rae, C. M., Florenchie, P., & Penven, P. (2006). 4 large scale physical variability of the Benguela current large marine Ecosystem (BCLME). *Large Marine Ecosystems*, *14*, 49–70. https://doi.org/10.1016/S1570-0461(06)80009-1

Siedlecki, S. A., Mahadevan, A., & Archer, D. E. (2012). Mechanism for export of sediment-derived iron in an upwelling regime. *Geophysical Research Letters*, *39*(3), L03601. https://doi.org/10.1029/2011GL050366

Steinfeldt, R., Sültenfuß, J., Dengler, M., Fischer, T., & Rhein, M. (2015). Coastal upwelling off Peru and Mauritania inferred from helium isotope disequilibrium. *Biogeosciences*, *12*(24), 7519–7533. https://doi.org/10.5194/bg-12-7519-2015

Stramma, L., & England, M. (1999). On the water masses and mean circulation of the South Atlantic Ocean. *Journal of Geophysical Research*, *104*(C9), 20863–20883. https://doi.org/10.1029/1999jc900139

Sunda, W., Huntsman, S., & Harvey, G. (1983). Photoreduction of manganese oxides in seawater and its geochemical and biological implications. *Nature*, *301*(5897), 234–236. https://doi.org/10.1038/301234a0

Tagliabue, A., Aumont, O., & Bopp, L. (2014). The impact of different external sources of iron on the global carbon cycle. *Geophysical Research Letters*, *41*(3), 920–926. https://doi.org/10.1002/2013GL059059

Tagliabue, A., Bowie, A. R., DeVries, T., Ellwood, M. J., Landing, W. M., Milne, A., et al. (2019). The interplay between regeneration and scavenging fluxes drives ocean iron cycling. *Nature Communications*, *10*(1), 1–8. https://doi.org/10.1038/s41467-019-12775-5

Thuróczy, C.-E., Boye, M., & Losno, R. (2010). Dissolution of cobalt and zinc from natural and anthropogenic dusts in seawater. *Biogeosciences*, *7*(6), 1927–1936. https://doi.org/10.5194/bg-7-1927-2010

Twining, B. S., & Baines, S. B. (2013). The trace metal composition of marine phytoplankton. *Annual Review of Marine Science*, *5*(1), 191–215. https://doi.org/10.1146/annurev-marine-121211-172322

Veitch, J., Penven, P., & Shillington, F. (2010). Modeling equilibrium dynamics of the Benguela current system. *Journal of Physical Oceanography*, *40*(9), 1942–1964. https://doi.org/10.1175/2010JPO4382.1

Ventura, A., Simões, E. F. C., Almeida, A. S., Martins, R., Duarte, A. C., Loureiro, S., & Duarte, R. M. B. O. (2021). Deposition of aerosols onto upper ocean and their impacts on marine biota. *Atmosphere*, *12*(6), 684. https://doi.org/10.3390/atmos12060684

Verhoef, A., Portabella, M., & Stoffelen, A. (2012). High-resolution ASCAT scatterometer winds near the coast. *IEEE Transactions on Geoscience and Remote Sensing*, *50*(7), 2481–2487. https://doi.org/10.1109/tgrs.2011.2175001

Vieira, L. H., Krisch, S., Hopwood, M. J., Beck, A. J., Scholten, J., Liebetrau, V., & Achterberg, E. P. (2020). Unprecedented Fe delivery from the Congo River margin to the south Atlantic Gyre. *Nature Communications*, *11*(1), 556. https://doi.org/10.1038/s41467-019-14255-2

Wallmann, K., José, Y. S., Hopwood, M. J., Somes, C. J., Dale, A. W., Scholz, F., et al. (2022). Biogeochemical feedbacks may amplify ongoing and future ocean deoxygenation: A case study from the Peruvian oxygen minimum zone. *Biogeochemistry*, *159*(1), 45–67. https://doi.org/10.1007/s10533-022-00908-w

Wu, M., McCain, J. S. P., Rowland, E., Middag, R., Sandgren, M., Allen, A. E., & Bertrand, E. M. (2019). Manganese and iron deficiency in Southern Ocean Phaeocystis antarctica populations revealed through taxon-specific protein indicators. *Nature Communications*, *10*(1), 1–10. https://doi.org/10.1038/s41467-019-11426-z

Xie, R. C., Galer, S. J. G., Abouchami, W., Rijkenberg, M. J. A., De Jong, J., De Baar, H. J. W., & Andreae, M. O. (2015). The cadmium-phosphate relationship in the western South Atlantic—The importance of mode and intermediate waters on the global systematics. *Marine Chemistry*, *177*, 110–123. https://doi.org/10.1016/j.marchem.2015.06.011

Xie, R. C., Rehkämper, M., Grasse, P., van de Flierdt, T., Frank, M., & Xue, Z. (2019). Isotopic evidence for complex biogeochemical cycling of Cd in the eastern tropical South Pacific. *Earth and Planetary Science Letters*, *512*, 134–146. https://doi.org/10.1016/j.epsl.2019.02.001

Yee, D., & Morel, F. M. M. (1996). In vivo substitution of zinc by cobalt in carbonic anhydrase of a marine diatom. *Limnology & Oceanography*, *41*(3), 573–577. https://doi.org/10.4319/lo.1996.41.3.0573

## References From the Supporting Information

Goddard Earth Sciences Data and Information Services Center (GES DISC). (2016). TRMM (TMPA) precipitation L31 day 0.25 degree × 0.25 degree V7. 2010. Retrieved from http://disc.sci.gsfc.nasa.gov/datacollection/TRMM_3B42_daily_V7.html

Wuttig, K., Townsend, A. T., van der Merwe, P., Gault-Ringold, M., Holmes, T., Schallenberg, C., et al. (2019). Critical evaluation of a seaFAST system for the analysis of trace metals in marine samples. *Talanta*, *197*, 653–668. https://doi.org/10.1016/j.talanta.2019.01.047